Seafloor chemosynthetic habitats and AOM-influenced sediment microbiome at a cold-water coral site off the Vesterålen coast, northern Norway

Claudio Argentino[1], Luca Fallati[2], Sebastian Petters[3], Hans C. Bernstein[3], Ines Barrenechea Angeles [1], Jorge Corrales-Guerrero[4], Alessandra Savini[2], Benedicte Ferré[1], Giuliana Panieri[1, 5]

[1] Department of Geosciences, UiT The Arctic University of Norway, 9037 Tromsø, Norway

[2] Department of Earth and Environmental Sciences, University of Milano-Bicocca, 20126 Milano, Italy

[3] The Norwegian College of Fishery Science, UiT The Arctic University of Norway, 9037 Tromsø, Norway

[4] Institute of Marine Research, 5005 Bergen, Norway

[5] Institute of Polar Sciences, National Research Council (CNR-ISP), 30172 Venice Mestre, Italy

Correspondence to: Claudio Argentino (claudio.argentino@uit.no)

Abstract. Cold seeps associated with cold-water corals have been reported worldwide. Yet, there are still knowledge gaps regarding ecological relationships due to contrasting observations. As a part of a larger multidisciplinary project on cold seeps off the Vesterålen coast (northern Norway), we~~Here, we report~~ analysed sediment (carbon-nitrogen systematics, foraminifera) and pore fluid (sulfate, dissolved inorganic carbon, methane) geochemistry and seafloor habitats (orthomosaics and habitat maps). ~~the results from a multidisciplinary study on cold seeps off the Vesterålen coast (northern Norway) hosting coral mounds. We discuss the geochemical results from sediment (carbon nitrogen systematics, foraminifera) and pore fluids (sulfate, dissolved inorganic carbon, methane) in relation to seafloor habitats (orthomosaics and habitat maps).~~ Microbial mats are the dominant seep-related community, forming white patches of a few ten cm in diameter, mostly distributed along the edges of methane-derived authigenic carbonates and on ~~cracks on top of them~~sedimented spots. Mats are associated with sulfate-methane transition zones as shallow as 5 cm and high production of ^{13}C-depleted dissolved inorganic carbon – evidence of ongoing anaerobic oxidation of methane. ~~Foraminifera tests in the sediment display negative δ^{13}C values down to − 18.5‰, suggesting ongoing authigenic carbonate precipitation.~~ We also report the discovery of a macroscopic white biofilm, observed while slicing a pushcore onboard. Organic matter analyses indicated that the sediment interval hosting this biofilm is associated with a sharp drop in δ^{13}C values, as negative as −43.4‰. Results from 16S rRNA gene analyses on the uppermost 10 cm in the same core showed a significant shift in microbial community. Protebacteria-dominated communities near the seafloor transition to a Halobacterota-dominated composition in correspondence of the biofilm interval, ~~mainly consisting of~~with amplicon sequence variants pointing to -ANME-1b anaerobic methanotrophs~~ in correspondence of the biofilm interval~~. The presence of a methane-charged sediment substrate leading carbonate crust formation, heterogeneous topography and food supply by high-energy currents appears to be a prerequisite for cold-water corals development and their spatial distribution in this area. Our results provide the biogeochemical and seafloor habitat context to CWCs, contributing to the understanding of potential influence of methane seepage~~s~~ on corals. Furthermore, the produced seafloor orthomosaics and habitat maps will facilitate the monitoring of habitat changes in response to future climate-driven environmental disturbances. ~~Corals in this area are spatially associated with seafloor chemosynthetic habitats and bubbling, but not vice versa, suggesting that seafloor emissions do not influence coral distribution. Instead, the presence of a methane-charged sediment substrate leading carbonate crust formation and food supply by high-energy currents appears to be a prerequisite for cold-water corals development in this area.~~

1 Introduction

Cold seeps are seafloor areas characterized by the emission of hydrocarbons, mostly methane, into the water column. These environments are found along continental margins worldwide (Phrampus et al., 2020) and typically support chemosynthetic communities that rely on chemical energy from reduced compounds (H_2S, CH_4) contained in the fluids (Joye, 2020). Their association with reef-building corals inhabiting deep (> 40 m) and cold waters, known as cold-water corals (CWCs), has been reported worldwide, i.e., from offshore New Zealand (Liebetrau et al., 2010), Gulf of Cadiz (Pirlet et al., 2012; Rincon-Tomas et al., 2019), Gulf of Mexico (Schroeder, 2002), South China Sea (Xu et al., 2019) and offshore Norway (Ferré et al., 2024; Hovland, 1990; Hovland and Thomsen, 1997). However, the biogeochemical relationships between cold seeps and CWCs remain unclear.

~~Reef building corals inhabiting deep (> 40 m) and cold waters are known as cold water corals (CWCs).~~ CWCs have been found at all continental margins, at water depths down to 3000 m and temperatures below 5 °C (Freiwald, 2011). They include a variety of scleractinian corals which do not rely on photosynthesis to produce energy, but feed on plankton and other organic particles transported by currents (Hovland, 2008a; Roberts et al., 2009). CWCs create a three-dimensional framework spanning tens of meters to ~~kilometers~~kilometres in lateral extent and up to 40 m in thickness (Freiwald, 2011; Sanna et al., 2023). It provides protective habitats for fish and other invertebrates, as well as a hard substrate for the settlement of other ~~sessile~~ organisms, i.e., foraminifera, hydrozoans, octocorals, serpulids, molluscs, bryozoans, brachiopods, and sponges (Freiwald, 2011). CWCs also represent nursery grounds and reproduction environments for commercial fish species (Husebø et al., 2002). Therefore, CWCs play a key role in deep-sea biodiversity and ecosystem functioning. Among them, *Desmophyllum pertusum* (known as *Lophelia pertusa*) is the most widespread and dispersed representative, very common in the North Atlantic (Roberts et al., 2009) and along the Norwegian coasts (Fosså et al., 2002; Sanna et al., 2023; Sundahl et al., 2020). It is known that besides adequate environmental conditions (temperature, food supplied by water current), CWCs require a hard substrate for colonization and growth of a large colony (Roberts et al., 2009). The substrate must be large and stable enough to resist strong currents. From that perspective, cold seeps would be optimal areas for their settling and growth as they are often associated with extensive carbonate pavements and/or mounds. During methane migration through the sediment, microbial communities consisting of methanotrophic archaea (ANME) and sulfate-reducing bacteria (SRB) (Boetius et al., 2000; Boetius and Wenzhöfer, 2013) carry out the anaerobic oxidation of methane (AOM) which is a globally widespread biofilter of this greenhouse gas (Egger et al., 2018; Lapham et al., 2024). AOM occurs in a relatively narrow zone within the sedimentary column, located at variable depths beneath the seafloor ranging from a few cm to several hundred meters, mainly depending on the magnitude of methane fluxes (Egger et al., 2018). Below the seafloor, sulfate is the quantitatively dominant electron acceptor available for microbes to oxidize methane, and sulfate-driven AOM releases bisulfide (HS^-) and dissolved inorganic carbon in the form of bicarbonate (HCO_3^-) following Eq. (1):

$$CH_4 + SO_4^{2-} \rightarrow HCO_3^- + HS^- + H_2O \quad (1)$$

$$HS^- + H_3O^+ \rightleftharpoons H_2S\,(aq) + H_2O \quad (2)$$

AOM-related sulfide fluxes (mainly in the form of H_2S under in situ conditions, Eq.2) toward the seafloor sustain chemosynthetic habitats, including chemosymbiotic mussels, clams, tubeworms, and microbial mats (Argentino et al., 2022b; Fischer et al., 2012; Sahling et al., 2002; Sen et al., 2018b). The protracted release of bicarbonate via AOM into pore water leads to an increase in alkalinity, which eventually triggers the precipitation of authigenic carbonates (Argentino et al., 2022a; Blumenberg et al., 2015; Crémière et al., 2016; Karaca et al., 2010). Methane-derived authigenic carbonates (MDAC) range from microscopic concretions to kilometerres-wide and several-meters-high deposits becoming exposed at the seafloor by winnowing and erosion (Argentino et al., 2019; Judd et al., 2020; Judd and Hovland, 2007; Tseng et al., 2023). MDAC outcrops are ideal places for the settling and growth of CWCs which benefit from optimal exposure to bottom currents rich in nutrients

(Rincon-Tomas et al., 2019). More recent studies suggested that CWCs can gain benefits not only from the presence of hard substrate (Deng et al., 2019; Rincon-Tomas et al., 2019; Xu et al., 2019) but also from chemosynthetically-derived food (Osman et al., 2023; Sert et al., 2025). Other studies found that the major food source in deep-sea corals is photosynthetically-derived food, even near cold seeps (Becker et al., 2009).

~~Ocean~~ Ocean acidification (OA) poses a potential threat to all coral reefs by reducing their growth rate (Kline et al., 2019) and inducing dissolution of their aragonitic skeletons (Eyre et al., 2018; Wisshak et al., 2012). Methane seeps can contribute to ocean acidification when methane (CH_4) is oxidized to carbon dioxide (CO_2) in the water column (Biastoch et al., 2011; Garcia-Tigreros et al., 2021; Hauri et al., 2024) following Eq. (3):

$$CH_4 + O_2 \rightarrow CO_2 + 2H_2O \quad (3)$$

~~However, compared to shallow water tropical corals, around 70 % of CWCs will be exposed to corrosive aragonite-undersaturated conditions in the course of this century, thus resulting in a dramatic loss of habitats and biodiversity (Bernardino et al., 2023; Hennige et al., 2014; Howes et al., 2015; Turley et al., 2007).~~ Conducting further investigations on cold seep biogeochemistry at CWC sites is needed, since the r~~R~~eduction of CWC ecosystems brings societal and economic implications, ~~offering new opportunities~~ in particular in the pharmaceutical, medical and food ~~research~~ industry (Beaumont et al., 2007; Foley et al., 2010; Hilmi et al., 2013).

~~Seafloor methane emissions, known as cold seeps, can contribute to ocean acidification when methane (CH_4) is oxidized to carbon dioxide (CO_2) in the water column (Biastoch et al., 2011; Garcia-Tigreros et al., 2021; Hauri et al., 2024) following Eq. (1):~~

~~$$CH_4 + O_2 \rightarrow CO_2 + 2H_2O \quad (1)$$~~

To respond to that call, ~~These seeps are widespread along continental margins (Phrampus et al., 2020) and their association with CWCs has been reported worldwide, i.e., from offshore New Zealand (Liebetrau et al., 2010), Gulf of Cadiz (Pirlet et al., 2012; Rincon-Tomas et al., 2019), Gulf of Mexico (Schroeder, 2002), South China Sea (Xu et al., 2019) and offshore Norway (Ferré et al., 2024; Hovland, 1990, p.199; Hovland and Thomsen, 1997, p.199). The causative link between the occurrence of CWCs and cold seeps has long been debated in the case of *Desmophyllum pertusum*(Hovland, 1990, p.199; Hovland and Thomsen, 1997). It is known that besides adequate environmental conditions (temperature, water current- food supply), CWCs require a hard substrate for colonization and growth of a large colony (Roberts et al., 2009). The substrate must be large and stable enough to resist strong currents. From that perspective, cold seeps are optimal areas as they are often associated with extensive carbonate pavements and/or mounds for their settling and growth. During methane migration through the sediment, microbial communities consisting of methanotrophic archaea (ANME) and sulfate reducing bacteria (SRB) (Boetius et al., 2000; Boetius and Wenzhöfer, 2013) carry out the anaerobic oxidation of methane (AOM) which is a globally widespread biofilter of this greenhouse gas (Egger et al., 2018; Lapham et al., 2024). AOM occurs in a relatively narrow zone within the sedimentary column, located at variable depths beneath the seafloor ranging from a few cm to several hundred meters, mainly depending on the magnitude of methane fluxes (Egger et al., 2018). Below the seafloor, sulfate is the quantitatively dominant electron acceptor available for microbes to oxidize methane and sulfate-driven AOM releases bisulfide (HS^-) and dissolved inorganic carbon in the form of bicarbonate (HCO_3^-) following Eq. (2):~~

~~$$CH_4 + SO_4^{2-} \rightarrow HCO_3^- + HS^- + H_2O \quad (2)$$~~

~~AOM-related sulfide fluxes (mainly in the form of H_2S) toward the seafloor sustain chemosynthetic habitats, including chemosymbiotic mussels, clams, tubeworms, and microbial mats (Argentino et al., 2022b; Fischer et al., 2012; Sahling et al., 2002; Sen et al., 2018b). The protracted release of bicarbonate via AOM into pore water leads to an increase in alkalinity, which eventually triggers the precipitation of authigenic carbonates (Argentino et al., 2022a; Blumenberg et al., 2015; Crémière et al., 2016; Karaca et al., 2010). Methane-derived authigenic carbonates (MDAC) range from microscopic concretions to kilometers-wide and several meters-high deposits becoming exposed at the seafloor by winnowing and erosion (Argentino et~~

~~al., 2019; Judd et al., 2020; Judd and Hovland, 2007, p.200; Tseng et al., 2023). MDAC outcrops are ideal places for the settling and growth of CWCs which benefit from optimal exposure to bottom currents rich in nutrients (Rincon-Tomas et al., 2019). More recent studies suggested that CWCs can gain benefits not only from the presence of hard substrate (Deng et al., 2019; Rincon-Tomas et al., 2019; Xu et al., 2019) but also from chemosynthetically-derived food (Osman et al., 2023; Sert et al., 2025). Other studies found that the major food source in deep-sea corals is photosyntheticallyderived food, even near cold seeps (Becker et al., 2009). These contrasting observations indicate that there are still knowledge gaps regarding the ecological relationships between seeps and CWCs.~~

~~I~~In 2022, ~~a~~A CWC-seep system offshore Vesterålen, Northern Norway, became the subject of the multidisciplinary project EMAN7 - *Environmental impact of Methane seepage and sub-seabed characterization at LoVe-Node 7* – aiming to investigate the interplay between CWCs and methane emissions. Within EMAN7 project, ~~in 2022~~ we conducted an expedition onboard RV Kronprins Haakon in summer 2022 (CAGE22-3, Ferré *et al.*, 2022) during which we also performed Remotely-Operated Vehicle (ROV) seafloor imagery acquisitions and targeted sediment samplings near *Desmophyllum pertusum* coral mounds. In this study, we combined the information obtained from seafloor orthomosaics and habitat maps with the geochemistry (pore fluids, organic matter, foraminiferal proxies) of shallow sediment cores. This multidisciplinary and multiproxy approach ~~to~~ enabled us to understand how methane spatial and temporal dynamics regulate the type and distribution of benthic habitats and subsurface carbon cycling. Moreover, we used 16S rRNA gene sequencing to explore downcore shifts microbial diversity and representative taxonomy through a push core showing the presence of a macroscopic white biofilm at 10 cm depth. ~~Our results~~This study provides a comprehensive overview of the biogeochemical context and seafloor environment ~~in which~~where the Vesterålen CWCs have developed, thus aiding in the assessment of ~~, that will serve both understanding of~~ the~~ir~~ potential influence of methane seepage on corals. Additionally, the generated seafloor orthomosaics and habitat maps will support the monitoring of habitat changes in response to future climate-induced environmental perturbations.~~current ecology and monitoring of the system response to future climate-induced environmental perturbations.~~

2 Study area

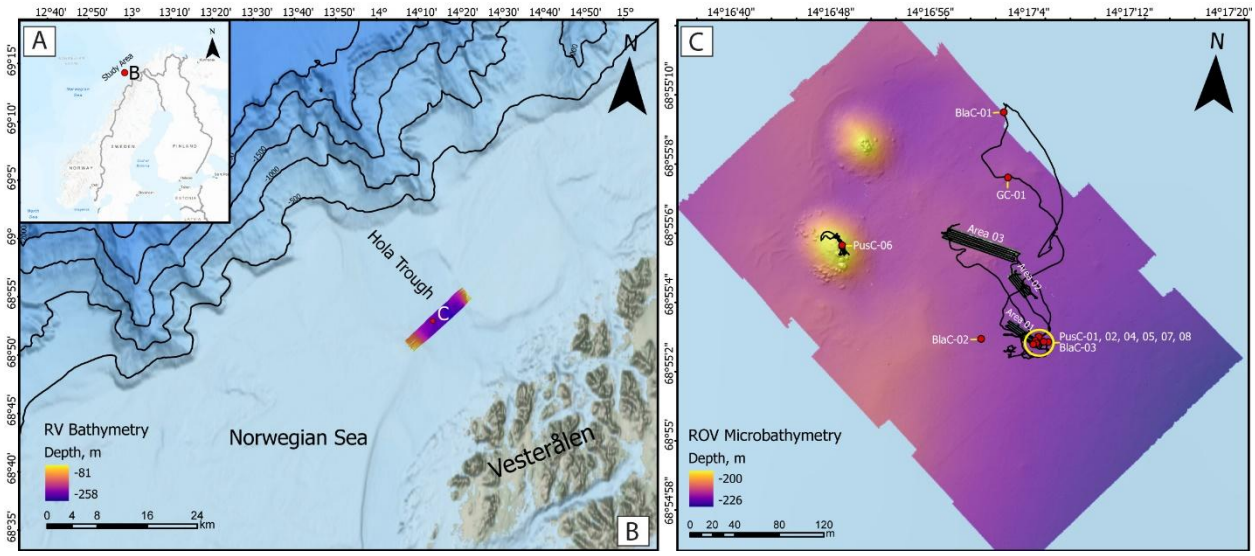

Figure 1. A) Geographical context of the study area located offshore Northern Norway. B) Bathymetric map of the Hola Through and Norwegian shelf off the Vesterålen islands. Ship-based multibeam bathymetry is shown with Viridis color palette accessible to people with color vision deficiencies. C) High-resolution ROV microbathymetry (Ferré et al., 2022, 2024) showing the sediment coring locations (red dots) and the three mosaic areas of Fig. 2. PusC-06 was excluded from analysis due to disturbance caused by reworking during sampling. Two CWC mounds marked by higher topography (yellow color) appear on the top-left corner. The ROV track is also displayed.

The targeted cold seeps investigated here are located on the Norwegian continental shelf at ~ 68.9 °N and ~ 14.3 °E (Fig. 1A), 15.5 km from the Vesterålen coast (Fig. 1B). This area is geomorphologically associated with the Hola Trough, an elongated ~12 km-wide depression carved by ice during Pleistocene glaciations (Ottesen et al., 2005). Water depths at the seep site range between 200 m and 230 m, and the seafloor is wiped by strong bottom currents up to 1 m s^{-1} (Ferré et al., 2024). CTD measurements conducted in 2023~~2~~2 during the cruise CAGE22-3 indicated water temperatures of 6.7 °C near the seafloor increasing to 8 °C at the sea surface, with salinity levels of 34-35 psu (Ferré et al., 2024). The seepage systems have been known since 2008 (Chand et al., 2008) and have been the focus of studies on hydrocarbon composition (Sauer et al., 2015) and seepage paleo-reconstructions (Crémière et al., 2016). The origin of the gas showed a predominantly thermogenic component, including methane with $\delta^{13}C_{CH4}$ values between −60‰ and −52‰ and δD_{CH4} between −225‰ and −191‰, associated with higher alkanes (C_{2+}) (Sauer et al., 2015). This gas migrates from late Jurassic to early Cretaceous source rocks and has been seeping since at least ~11 ka (Crémière et al., 2016), producing extensive ~~methane-derived carbonate (~~MDAC~~)~~ pavements. The Hola Trough is of great biological interest due to the presence of more than 300 *Desmophyllum pertusum* reefs distributed over an area of almost 50 km^2 with individual reefs having heights up to 17 m and widths > 300 m in the longest direction (NNW-SSE; Bøe *et al.*, 2016). In the investigated seepage area ~~(Fig. 2C),~~ CWCs form two main mounds (appearing on the left side of the microbathymetry in Fig. 2C) but minor coral build-ups are also present over a larger area hosting gas seeps (Ferré et al., 2022, 2024)~~two coral mounds appear on the left side of the microbathymetry~~. The ROV survey performed during CAGE22-3 (Ferré et al., 2022) enabled high-resolution seafloor mosaicking, habitat mapping, and video-guided coring at specific microhabitats. ~~These efforts aimed to support biogeochemical investigations focused on reconstructing methane dynamics and understanding its influence on seafloor ecosystems near CWCs.~~

3 Methods

3.1 Seafloor ROV video acquisition and Structure from Motion processing

Seafloor imagery was collected in 2022 during the CAGE22-3 cruise ~~aboard R/V *Kronprins Haakon* ~~(Ferré et al., 2022). During the second ROV dive of the cruise, three sub-areas (Area 01, Area 02, Area 03) were surveyed using high-resolution video acquisition for photogrammetric mosaicking (Fig.1-C). ~~These sites are characterised by extensive carbonate crusts interspersed with microbial mats.~~ They were selected based on intense seep activity previously identified ~~through~~ by screening the water column ~~analyses~~ for gas flares (high backscatter) using R/V-mounted multibeam echosounder (MBES) data (Ferré et al., 2024). ~~This analysis enabled the detection of acoustic flares, indicative of gas seepage from the seafloor, as well as the mapping of their spatial distribution in relation to bathymetric features.~~

ROV Ægir 6000, a 150 Hp work-class vehicle equipped with various samplers and sensors and operated by the Norwegian Marine Robotics Laboratory (NORMAR) at the University of Bergen (UiB), was deployed with an EM 2024 Kongsberg MBES mounted on it and a dedicated photogrammetry sledge.

The MBES was used to create a high-resolution microbathymetric map of the surveyed region (Fig. 1). Mounted on the ROV, this MBES captures detailed topographic data at sub-meter to decimet~~e~~rre scales, offering essential context for interpreting seafloor features in the imagery and improving the spatial precision of photogrammetric outputs.

The photogrammetry sledge included a downward-facing Imenco® Spinner II Shark HD zoom camera mounted perpendicular to the seafloor. Illumination was provided by two high-output strobes (>2500 W) and a pair of deep-sea power lasers spaced 14 cm apart, ensuring consistent lighting and enabling scale calibration. ROV video acquisition, with the downward-facing camera, was conducted along parallel transects spaced 2 m apart, with the ROV maintaining a steady speed of 0.3 knots and an altitude of 2.5 m. This configuration resulted in a field of view slightly greater than 2 m and ensured sufficient image overlap for photogrammetric reconstruction. These acquisition parameters were validated in previous field campaigns (Fallati et al.,

2023; Panieri et al., 2024). In total, four ~35 m transects were collected in Area 01, five ~30 m transects in Area 02, and six ~60 m transects in Area 03.

ROV positioning for both MBES and photogrammetric surveys was achieved using the HIPAP 501 USBL (Ultra Short Baseline) system, ensuring high-precision localisation. These positional data were later integrated into the geospatial processing workflow to scale and georeference the resulting models accurately.

ROV videos were processed by automatically extracting one frame per second using VLC Media Player's Scene Video Filter, producing high-definition (1920 × 1080 px) PNG images sorted by survey area. These images were imported into Agisoft Metashape Professional 2.0 (Agisoft, 2018) and processed following a standard Structure from Motion (SfM) workflow (Fallati et al., 2020; Lim et al., 2020; Montes-Herrera et al., 2024; Price et al., 2019). After camera alignment, dense point clouds were generated to produce ultra-high-resolution digital elevation models (DEMs) and orthomosaics. The spacing between the laser pointers served as a ground-truth scale bar for each model.

To georeference the models, USBL-derived coordinates and timestamps were linked to selected video frames, primarily those at the ends and centres of each transect. These data points were further cross-validated against geomorphic features visible in both the ROV-derived microbathymetry and the SfM-generated DEMs. This multisource integration enabled the accurate spatial placement of the models within the WGS 84 / UTM Zone 33N coordinate system.

Substrate semi-automatic classification was performed using Object-Based Image Analysis (OBIA) in the eCognition Developer (Trimble) environment. This approach segments the orthomosaics into meaningful image objects based on spectral, textural, and spatial characteristics (Benz et al., 2004; Blaschke, 2010; Hay and Castilla, 2008; Hossain and Chen, 2019), allowing for the supervised classification of distinct substrate classes, such as ~~methane-derived authigenic carbonate crust (MDAC)(Crémière et al., 2016; Sauer et al., 2017),~~ fine-grained sediments mixed with gravels and pebbles, microbial mats, boulders, and benthic organisms. The interpretation of the observed hardgrounds as MDAC pavements was based on previous extensive studies at this site which reported low $\delta^{13}C$ values for these materials ranging from −38.0‰ to −22.2‰ and the incorporation of biomarkers typical of AOM-performing microbial consortia (Crémière et al., 2016; Sauer et al., 2017).

3.2 Sediment coring

Sediment samplings near the mounds and adjacent sediment were hindered by the presence of a stiff layer of coral debris and/or hardgrounds partially exposed at the seafloor. Moving away from the mounds, we managed to obtain cores for biogeochemical investigations and decided to focus on these areas for samplings and orthomosaicking. Six push cores, three blade cores, and one gravity core ~~(Fig. 1C~~ were collected during the expedition CAGE22-3 (Ferré et al., 2022) (Fig. 1C). ~~.~~ The blade corer consisted of a 32 cm-long frame with a rectangular base of 25 x 10 cm. It was pushed into the seabed using the ROV manipulator arm and a locking system was activated to avoid sample loss. This technique is especially suitable for coarse-grained sediments. We collected three blade cores CAGE22-3-KH-01-BlaC-01, CAGE22-3-KH-01-BlaC-02, and CAGE22-3-KH-01-BlaC-03, hereafter named BlaC-01, BlaC-02 and BlaC-03, respectively. BlaC-01 was collected as a reference core for geochemical interpretations from a seafloor spot barren of chemosynthetic fauna (Ferré et al., 2022). BlaC-02 and BlaC-03 were collected from microbial mats. We also conducted push coring using a 60 cm-long cylindrical tube (8 cm inner diameter) made of fiberglass. The push corer was pushed into the sediment by the ROV during samplings and enabled us to obtain longer cores. We collected six push cores: CAGE22-3-KH-01-PusC-01, CAGE22-3-KH-01-PusC-02, CAGE22-3-KH-01-PusC-04, CAGE22-3-KH-01-PusC-05, CAGE22-3-KH-01-PusC-07 and CAGE22-3-KH-01-PusC-08, hereafter named PusC-01, PusC-02, PusC-04, PusC-05, PusC-07 and PusC-08, respectively and all collected from microbial mats. We also report the data from gravity corer CAGE22-3-KH-01-GC-01 (GC-01), which was collected using a 6-m-long iron barrel hosting a PVC liner with an inner diameter of 10 cm. On deck, the cores were split into 1-m-long sections (or shorter depending on the recovery), capped, labelled, and stored at 4 °C. Pore fluid analyses were conducted on all the cores, whereas PusC-08

and BlaC-01 were selected for sediment geochemistry and foraminifera analyses. Preliminary microbiological analyses were only performed on PusC-08, due to the discovery of a biofilm at 10 cm.

3.3 Pore fluid samplings and analyses (CH_4, SO_4^{2-}, DIC, $\delta^{13}C_{DIC}$)

Pore water extractions were conducted in a cold room (4 °C) immediately after coring operations. We sampled every 2 cm using rhizon soil moisture samplers (5 cm-long filter; 0.15 µm mesh) and 10 mL sterile plastic syringes. We split the pore water samples into two aliquots: one aliquot for dissolved inorganic carbon (DIC) analyses was transferred into 2 mL glass scintillation vials to which we added 10 µL of $HgCl_2$ saturated solution. DIC samples were then stored in the dark at 4 °C; the other aliquot for sulfate analysis was transferred into 5 mL Eppendorf tubes and stored at −20 °C. DIC concentrations and isotopic composition ($\delta^{13}C$) were measured on a Thermo Fisher Scientific MAT 253 IRMS coupled to a Gasbench II at the Stable Isotope Laboratory (SIL) of the Department of Geosciences, UiT. Isotopic values were normalized to Vienna Pee Dee Belemnite standard (VPDB) using three in-house calcite reference materials covering a $\delta^{13}C$ range from −48.95‰ to 1.96‰. DIC concentration was calculated by comparing the IRMS peak areas for the samples with calibration curves made from two $NaHCO_3$(aq) stock solutions. Repeatability precision (1s) of $\delta^{13}C$ and DIC concentration based on ~~five~~ three duplicate samples was better than or equal to 0.23‰ and 1.2 mM, respectively. The sulfate concentration was measured via ion chromatography at TosLab in Tromsø (NO). Accuracy and precision were estimated based on repeated measurements of certified materials. The measured values agreed within the uncertainty of the certified value and are commonly associated with a precision of 15% (relative standard error RSE). Bulk sediment samples were collected from the bottom of push cores and from depths ranging from 5 to 15 cm in blade cores using a cut-off syringe. Around 5 mL of sediment were transferred to 20 mL serum vials containing two glass beads and 5 mL of 1 M NaOH. The vials were immediately closed with a rubber septum and aluminum crimp seal and stored upside-down at 4 °C. Methane concentration was measured on a Thermo Fisher Scientific GC Trace 1310 gas chromatograph at the SIL laboratory.

3.4 Benthic foraminifera isolation and isotope analyses ($\delta^{13}C$, $\delta^{18}O$)

We conducted down-core foraminiferal investigations in PusC-08 (microbial mat microhabitat) and in reference core BlaC-01. The isotopic composition of foraminifera was used to trace MDAC precipitation as secondary overgrowth. We combined foraminifera geochemistry with pore water data to determine whether isotopic anomalies in foraminifera are associated with modern or ancient Sulfate-Methane Transition Zones (SMTZ). Push core PusC-08 and blade core BlaC-01 were sliced onboard every cm. For each sample, we weighed around 50 g of dry sediment and wet-sieved it through 63 µm and 125 µm sieves. We dried the residue at 50 ˚C and hand-picked benthic foraminifera with identification at genus or species level. Picking was conducted from the fraction >125 µm using a stereomicroscope. From each aliquot we selected a number of individuals ranging from 5 to 15 for isotope analysis. The dominant species in most of the samples were *Cibicidoides lobatulus* and~~,~~ *Cassidulina spp*~~. and *Trifarina spp*~~. Some of the samples were barren of these target foraminifera, thus resulting in a total of 41 and 13 samples for PusC-08 and BlaC-01, respectively. Isotope analyses were conducted at the SIL laboratory using a Thermo Fisher Scientific MAT 253 IRMS with a Gasbench II. Precision on two replicate reference materials (n = 6) was better than 0.1‰ for both carbon and oxygen. All isotope results were normalized to Vienna Pee Dee Belemnite standard (VPDB) using three in-house reference materials ranging in $\delta^{13}C$ and $\delta^{18}O$ from –48.95‰ to 1.96‰ and from −18.59‰ to −2.15‰, respectively.

3.5 Sediment chemical analyses (TOC, TN_d, $\delta^{13}C_{org}$, $\delta^{15}N_d$)

We conducted geochemical investigations of the organic matter ~~on~~ in ~~the~~ core PusC-08 ~~containing a biofilm described below and shown in Fig 5A,~~ and ~~reference core~~ BlaC-01 to identify the presence of methanotrophic biomass in the sediment. In combination with pore water data, it is possible to discriminate between modern or ancient AOM-impacted intervals. Negative $\delta^{13}C_{org}$ values lower than the ranges for marine and terrestrial end-members can be used as a proxy for AOM-associated microbial biomass in the sediment (Argentino et al., 2023, 2024; Ghosh et al., 2025; Szymczycha et al., 2025).We ~~and~~ analysed a total of 45 sediment samples from PusC-08 and 15 samples from BlaC-01 collected every cm down the cores. Prior to the analyses, the samples were treated with 6 N HCl to remove the carbonate component following the protocol reported in Argentino *et al.* (2023). ~~Decarbonated material was analyzed~~Analyses were conducted on~~using~~ a Thermo Fisher Scientific MAT 253 Isotope Ratio Mass Spectrometer (IRMS) coupled to a Flash HT Plus Elemental Analyzer hosted at the SIL laboratory. The $\delta^{13}C$ and $\delta^{15}N$ values were obtained by normalization to international standards, Vienna Pee Dee Belemnite, VPDB ($\delta^{13}C$) and Air-N_2 ($\delta^{15}N$), using three in-house reference materials ranging in $\delta^{13}C$ and $\delta^{15}N$ from –40.44‰ to –9.14‰ and from −4.91‰ to 20.73‰, respectively. The total nitrogen in the decarbonated material (TN_d) is hereafter assumed to represent organic nitrogen based on the close-to-zero-intercept of TN_d versus total organic carbon (TOC) for TOC = 0 (e.g. Knies et al., 2007). This assumption allowed us to consider TN_d values as mixtures of different organic sources, and the bulk nitrogen isotopic composition ($\delta^{15}N_d$) can be used for organic source interpretations (Argentino et al., 2023; Hu et al., 2020). Repeatability precision (1s) of four duplicate samples measured in the same analytical session was better than or equal to 1.7‰, 0.12 %, 0.66‰, and 0.011 % for $\delta^{13}C_{org}$, TOC, $\delta^{15}N_d$, TN_d ~~(total nitrogen in the decarbonated material)~~, respectively. The C/N_d atomic ratio was calculated using the atomic mass weighted ratio of TOC and TN_d as C/N_d = (TOC/12.011)/(TN/14.007). The precision (1s) on C/N_d values was better than 0.65.

3.6 DNA extraction and sequencing

Sediment samples for DNA analyses were collected from PusC-08 immediately after core recovery using sterile spoons and stored frozen at −80 °C until processing. Samples were collected every cm in the interval 0-10 cm. For DNA extraction, 0.2-0.5 g of sediments was extracted using the DNeasy Power Soil Kit (Qiagen, Carlsbad, CA) and stored at −80 °C. DNA quality was measured by a NanoDrop Spectrophotometer and a Qubit Fluorometer (Invitrogen). The V4 region of the 16S SSU rRNA gene was amplified following the Earth Microbiome Project (EMP) (Gilbert et al., 2014) 16S Standard191Illumina library preparation protocol, using the forward-barcoded 515f (5'-3'192GTGYCAGCMGCCGCGGTAA) and 806r (5'-3' GGACTACNVGGGTWTCTAAT). The quality of PCR products was assessed using 1 % agarose gel electrophoresis and GelRed staining, and three replicates per sample were chosen for sequencing. Illumina MiSeq sequencing was performed at the Environmental Sample Preparation and Sequencing Facility at Argonne National Laboratory (Lemont, IL, USA). The amplicon analyses were performed with the QIIME2 environment and using QIIME2 plugins as previously described in Aalto *et al.*(2022). Briefly, Illumina forward and reverse reads and the corresponding barcode files were imported and demultiplexed using the Earth Microbiome Project paired-end flag. All reads were quality filtered, de-replicated, and chimera-checked using all default parameters in DADA2 v2021.2.0 (Callahan et al., 2016). The reads were merged and amplicon sequence variants (ASVs) were determined using DADA2 v2021.2.0. The DADA2 statistic on sequence reads is provided in Data set S1. A 16S from the SILVA v138.1 database was trained using RESCRIPt (Quast et al., 2013; Robeson et al., 2021). The ASVs were classified with the self-trained classifier database (Yilmaz et al., 2014). Sequences are being processed for archiving with the European Nucleotide Archive and ~~will~~are ~~be~~ available under accession PRJEB96327.

3.6.1 Statistical analyses

All ASVs not assigned to the expected kingdom (Archaea and Bacteria) were removed. Downstream analysis was completed in R (R Core Team, 2021), using the `microeco´ v0.11.0 (Liu et al., 2021) -and `vegan´ v2.5-7 packages (Oksanen et al., 2001). In particular, the R packages were used to calculate relative organismic abundances, observed alpha diversity, beta diversity using unweighted UniFrac, PERMANOVA, and Pearson correlation.

4 Results

4.1 Orthomosaics and benthic coverage maps

~~The morphobathymetric map produced from the ROV MBES data revealed a more complex area compared to the relatively level surrounding seafloor.~~ The three orthomosaics (Fig. 2, A1, A2, A3), generated at millimetric resolution, cover a total area of 1,307 m² and generally show a hard seafloor composed of compact patches of MDAC, colonized by numerous benthic organisms, such as sponges, sea anemones, and sea fans. Outside the MDAC areas, the seafloor is characterized by fine sediments mixed with gravels and pebbles, which dominate the mapped area and include coral rubble.

The high resolution of the orthomosaics enabled the detection and mapping of small, subcircular microbial mat patches, mainly found along the edges of the carbonate crusts (Fig. 2, C1, C2, C3). These patches vary in surface area from 0.002 to 0.17 m², with an average of 0.02 m² and an average perimeter of 0.58 m.

OBIA-derived benthic coverage maps identify the main seafloor classes in the high-resolution orthomosaics. Area 1 (Fig. 2, A1-B1), covering 312 m², primarily consists of fine sediments with gravels, occupying about 267 m². Microbial mats are located near the carbonate crusts (4.6 m²) in the south-central part of the area, with a total surface area of 0.26 m². In the area, two benthic nodes (landers) are present, and well visible in the orhomosaic (Fig. 2, A1) as part of the project LoVeOcean, Lofoten-Vesterålen Ocean Observatory (https://loveocean.no/).

Area 2 is smaller (Fig.2, A2-B2), at 258 m², and features a central, slightly elevated subcircular MDAC patch (42.2 m²), surrounded by fine sediments with gravels and pebbles (211 m²). This area also displays a more complex three-dimensional structure and hosts numerous benthic organisms and small microbial mat patches, which together cover 0.22 m².

Area 3 comprises the largest portion of the mapped seafloor (Fig. 2, A3-B3), spanning 738 m². Most of this area is dominated by fine sediments with gravels (437.7 m²), along with extensive, discontinuous MDAC outcrops (282 m²) concentrated in the northwestern section. Small, subcircular bacterial mats are also visible along the rims of the carbonate crusts, with a total surface coverage of 1.65 m².

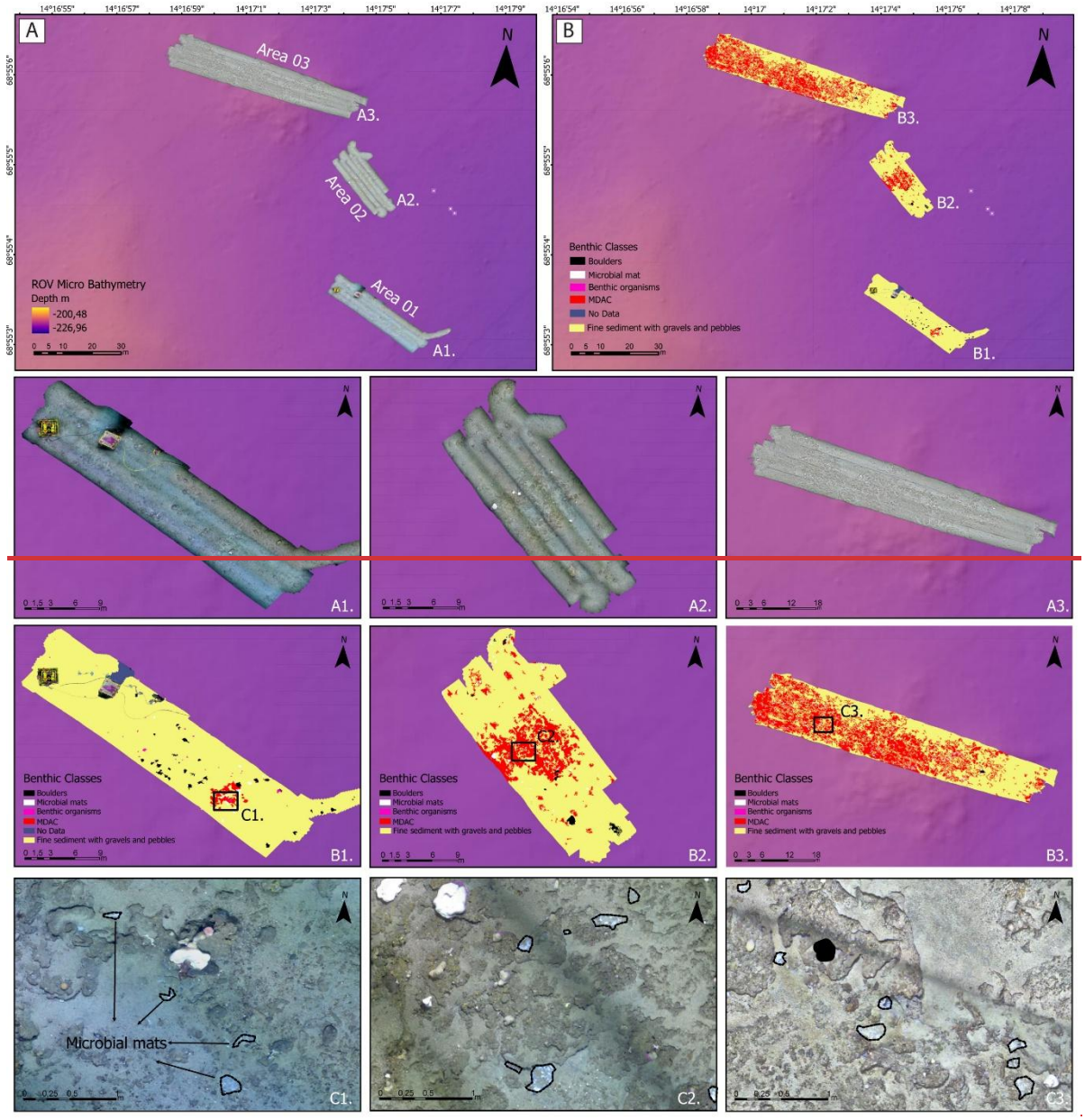
A
Area 03
A3.
Area 02
A2.
Area 01
A1.
ROV Micro Bathymetry
Depth m
-200,48
-226,96
B
B3.
B2.
B1.
Benthic Classes
Boulders
Microbial mat
Benthic organisms
MDAC
No Data
Fine sediment with gravels and pebbles
C1.
C2.
C3.
Microbial mats

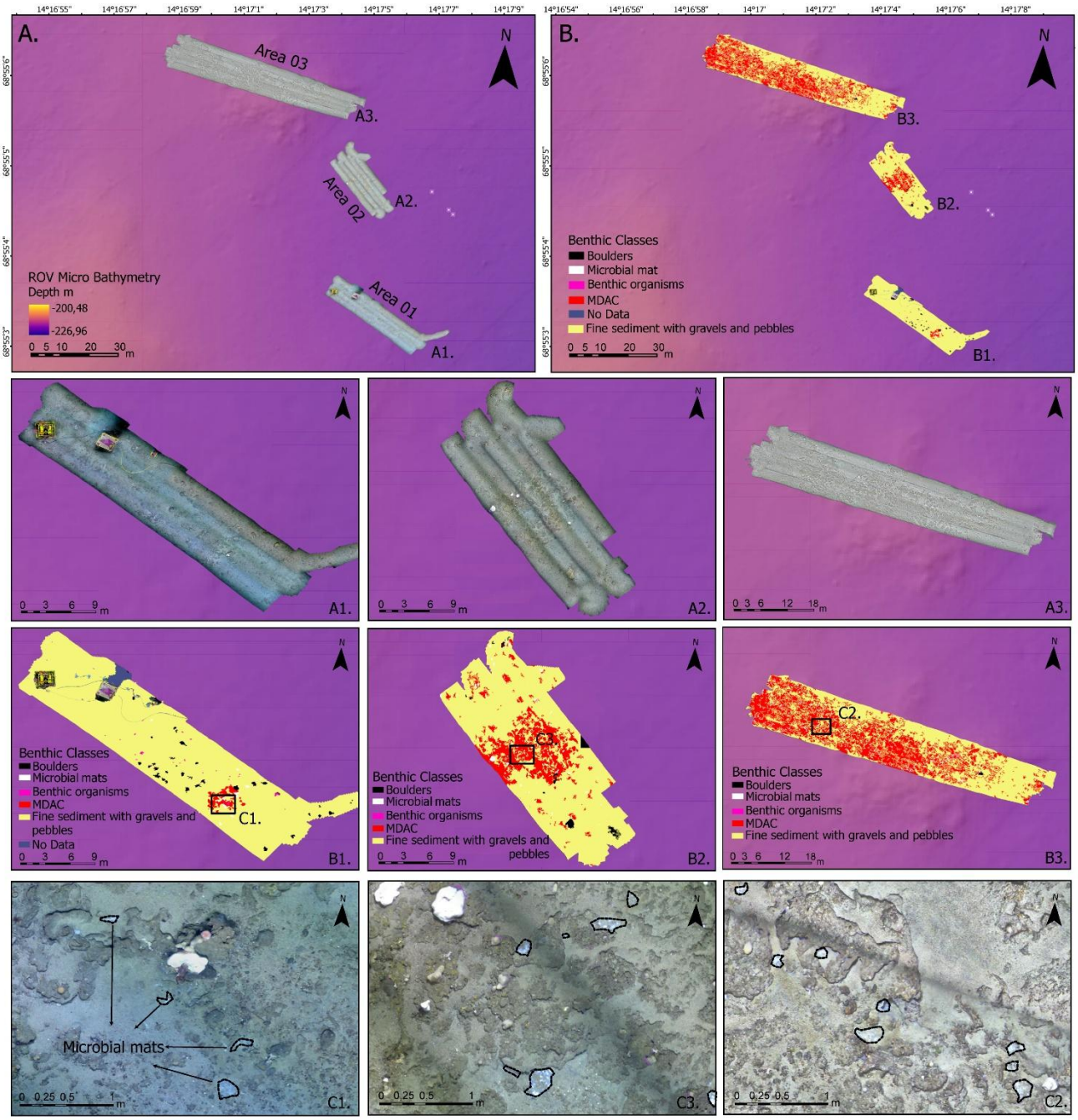

345 **Figure 2. A. Close-up of the microbathymetry area with high-resolution orthomosaics of the three surveyed subareas (Area 1, Area 2, Area 3). B. Benthic coverage maps produced through OBIA showing the seafloor composition and distribution of methane-derived authigenic carbonate crusts (MDAC), fine sediments with gravels and pebbles, benthic organisms, and microbial mat patches. The analysis of the orthomosaics (A1, A2, A3) and the benthic coverage maps (B1, B2, B3) reveal subcircular microbial mats~~, primarily~~ located ~~along the margins of the~~near MDAC outcrops (C1, C2, C3). For a better view of small-scale features, we recommend**
350 **accessing the dataset at https://doi.org/10.18710/1FCVAE.**

4.2 Pore water geochemistry and methane concentration

All pore water profiles from the 10 investigated cores are reported in the Supplement (Fig. S1)~~, while t~~. Two cores were selected based on completeness of the data (no gaps in either sulfate or DIC profiles) to discuss the subsurface biogeochemistry
355 of microbial mats (Fig. 3). Sulfate concentration~~s~~ in surface sediments (0-1 cm below the seafloor) ~~varie~~varies from a normal seawater ~~composition~~ value ~29 mM (Millero, 2005) to as low as 24.3 mM (PusC-01; presence of a microbial mat at the seafloor). Sulfate values < 1 mM are observed in two cores, PusC-02 (Fig. S1) and PusC-04 (Fig. 3), at 24 cm and 10 cm,

respectively ~~(Fig. 3)~~. ~~Downcore concentration profiles in the investigated cores include concave-up (PusC-01, PusC-04, PusC-08), concave-down (GC-01), quasi-linear (PusC-05, BlaC-01, BlaC-02, BlaC-03) shapes (Fig. 3), and two kink-type profiles (PusC-02 and PusC-07).~~ Concentrations of dissolved inorganic carbon ~~Dissolved inorganic carbon~~ in surface sediments (0-1 cm) ranges from 2.2 mM (BlaC-01) to 5.1 mM (PusC-01), with overall increasing downcore trends (Fig. S1). ~~The steepest gradients occur starting at ~5 cm in PusC-02, between 2-6 cm in PusC-04 and 15-31 cm in PusC-07. The other cores have low or quasi-zero sulfate gradients throughout the sampled depths.~~ DIC isotopic composition ($\delta^{13}C$) in surface sediment ranges from −22.5‰ (PusC-01) to −1.1‰ (BlaC-01) (Fig. S1). Isotopic values decrease with depth, with the most negative value $\delta^{13}C$ = −29.8‰ measured at 6 cm in PusC-04 and at 18 cm in PusC-08, which also corresponds to an inversion in isotopic trends (becoming ~~heavier~~ higher down the core). Methane concentration in samples collected from the bottom of the push cores and at 5-15 cm in blade cores are reported in the Supplement (Table S1). ~~-~~Methane concentrations ~~in the push cores range from~~show high values in pushcores, ranging 1.2 mM (PusC-02) to 3.4 mM (PusC-04)~~.~~, ~~whereas blade~~Blade cores contain trace amounts of methane, with measured values of 0.003 mM (BlaC-01; 10 cm depth), 0.010 mM (BlaC-02; 5 cm depth) and 1.1 mM (BlaC-03; 15 cm depth).

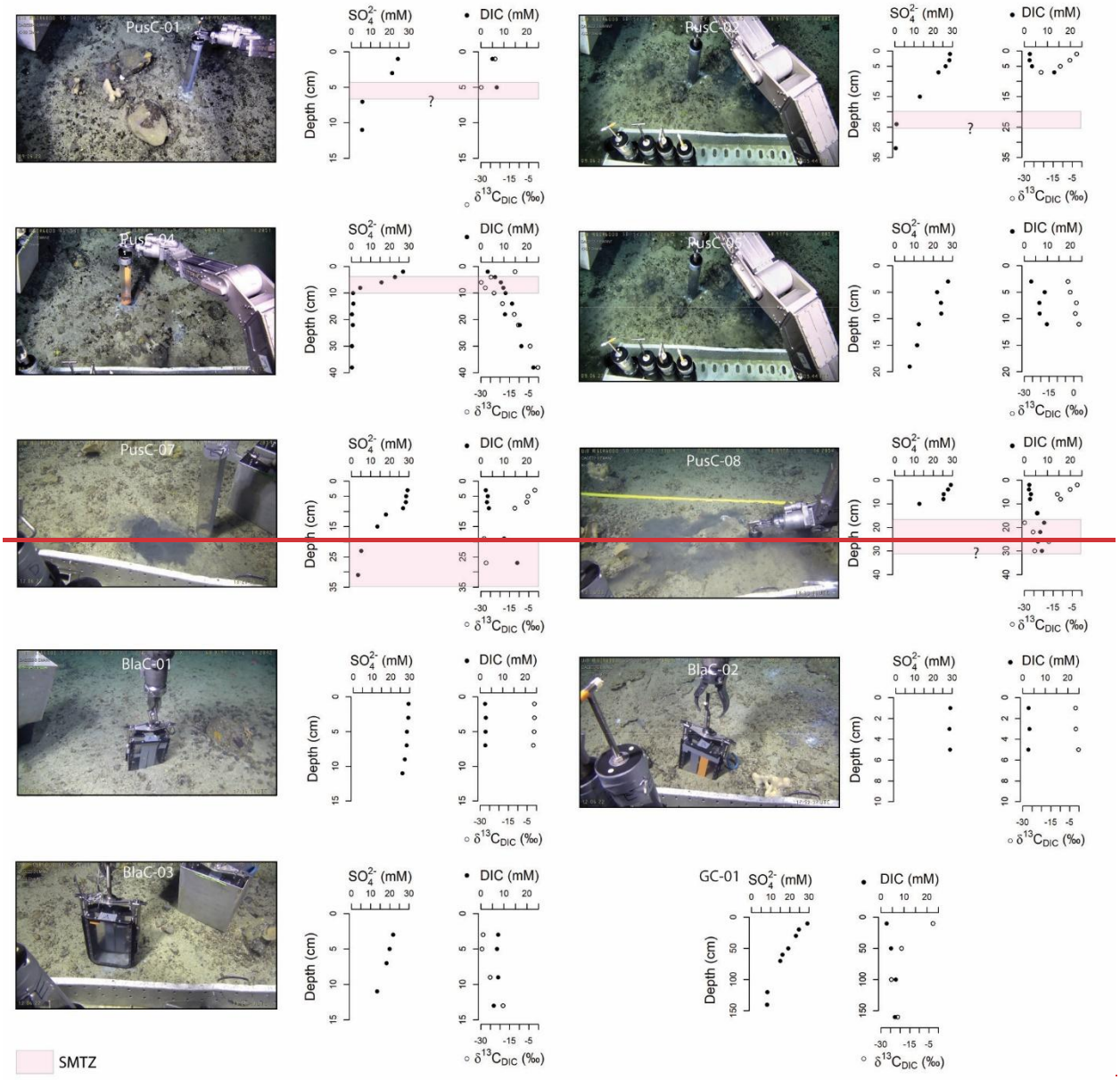
PusC-01
PusC-02
PusC-04
PusC-06
PusC-07
PusC-08
BlaC-01
BlaC-02
BlaC-03
GC-01
SO4 2- (mM)
DIC (mM)
Depth (cm)
δ13CDIC (‰)
?
SMTZ

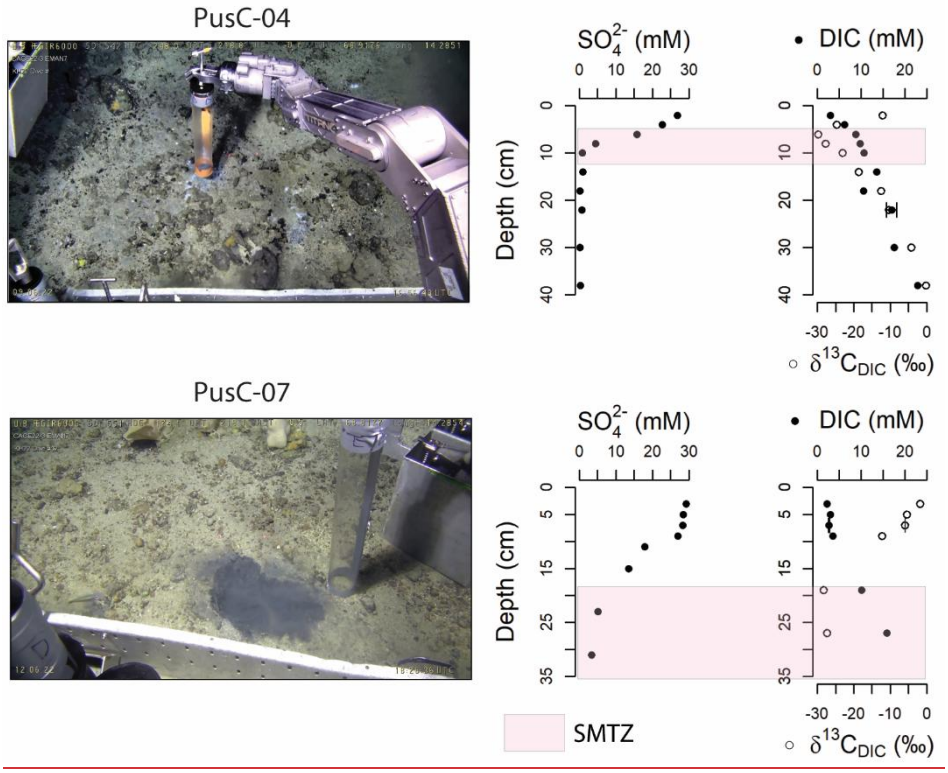

Figure 3. Seafloor images and pore water geochemical profiles of selected sediment cores collected from the CWC area. Locations in relation to cold water coral mounds is shown on the microbathymetry of Fig. 1C and on the mosaics and habitat maps of Fig. 2. The ~~sulfate-methane transition zone (~~SMTZ~~)~~ is marked with pink color ~~and identified in correspondence of~~in concomitance of a drop in sulfate concentrations and $\delta^{13}C_{DIC}$, and an increase~~s~~ in DIC concentrations. Pore water profiles for all the investigated cores are reported in Fig. S1. Error bars refer to standard uncertainty and correspond to one standard deviation.

4.3 Foraminifera geochemistry

The carbon isotopic composition $\delta^{13}C$ of *Cibicidoides lobatulus* and~~,~~ *Cassidulina spp.* ~~and *Trifarina spp.*~~ shows a marked difference between reference core BlaC-01 and PusC-08. In BlaC-01, $\delta^{13}C$ values in *Cibicidoides lobatulus* and *Cassidulina spp.* range~~s~~ from 0.8‰ to 1.9‰, and ~~-~~from −1.5‰ to −1.0‰ ~~and from 0.3‰ to 0.9‰~~, respectively. In push core PusC-08, the same categories of foraminifera show values from − 18.5‰ to 1.7‰ and~~,~~ from −15.0‰ to 1.0‰ ~~and from −0.1‰ to 1.0‰~~. In the blade core, *Cibicidoides lobatulus* and~~,~~ *Cassidulina spp.* ~~and *Trifarina spp.*~~ have $\delta^{18}O$ values within the intervals 2.4-3.5‰ and~~,~~ 4.1-4.3‰ ~~and 2.3-2.7‰~~. In PusC-08, the range of $\delta^{18}O$ values are 2.0-4.1‰ and~~,~~ 1.8-4.6‰ ~~and 1.7-2.9‰~~. BlaC-01 displays rather flat downcore isotope profiles (Fig. 4A), while PusC-08 shows a sharp increase in $\delta^{18}O$ and decrease in $\delta^{13}C$ starting at 20 cm below the seafloor (Fig. 4B).

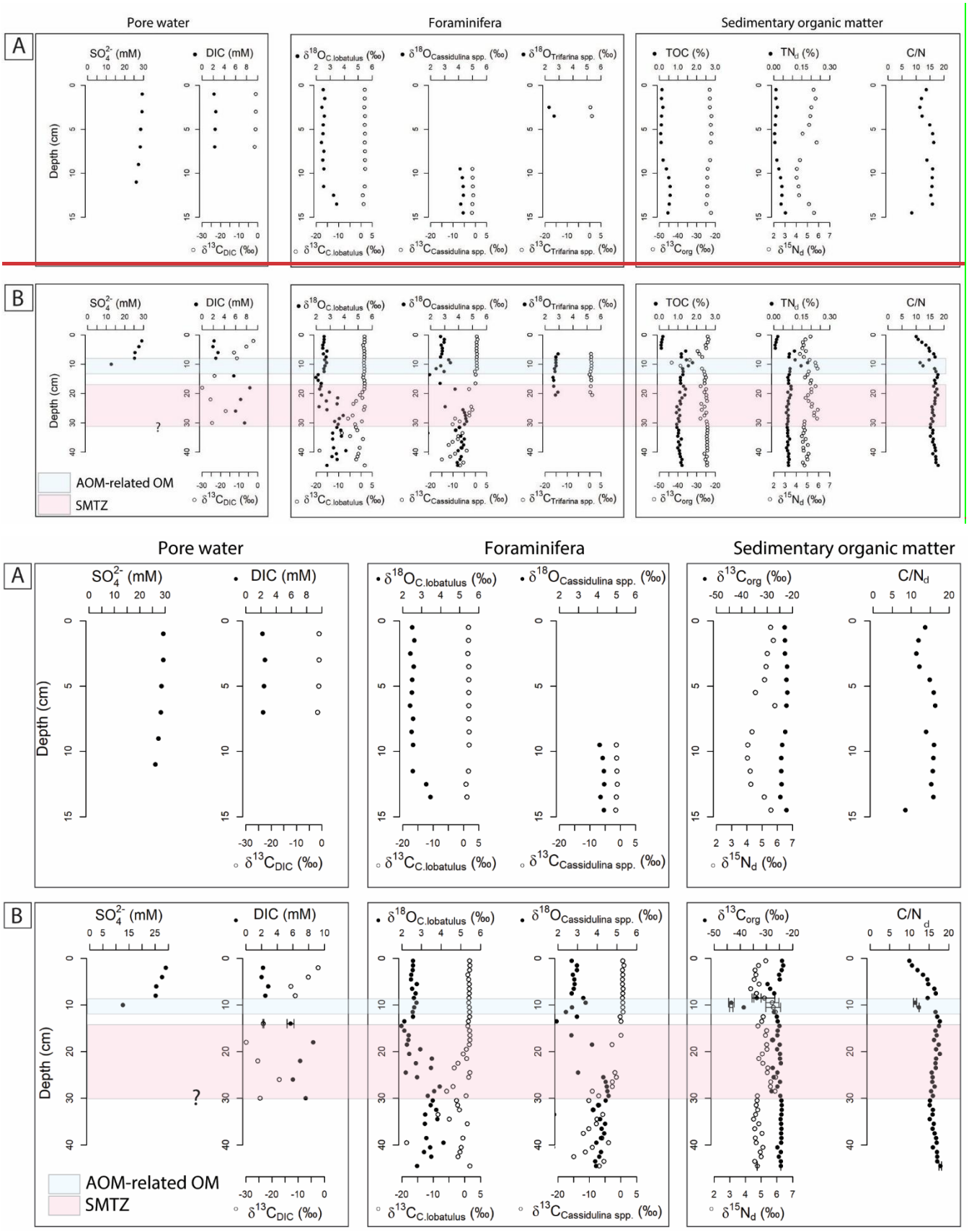

Figure 4. Pore water, foraminifera and sediment geochemical profiles of reference core BlaC-01 (A) and PusC-08 (B). The SMTZ is marked with pink color in PusC-08, whereas it has not been intercepted in BlaC-01. Question mark at the base of the SMTZ indicates uncertainty on the interpretation of its thickness due to missing pore water data below 30 cm. We marked in blue color the interval containing AOM-related organic matter in PusC-08, as determined by carbon-nitrogen interpretations (see full text). Error bars refer to standard uncertainty and correspond to one standard deviation.

4.4 Carbon-nitrogen geochemistry

~~TOC~~ The contents of total organic carbon in BlaC-01 range from 0.07 % to 0.58 % and are associated with $\delta^{13}C_{org}$ values from −24.8‰ to −22.1‰. TN_d contents range from 0.01 % to 0.06 %, with isotopic values $\delta^{15}N_d$ between 4.1‰ and 5.8‰. The resulting C/N_d values range from 8.5 to 16.3. PusC-08 has TOC contents ranging from 0.09 % to 1.78 %, associated with $\delta^{13}C_{org}$ values from −43.4‰ to −23.6‰. TN_d and $\delta^{15}N_d$ varies between 0.01 % and 0.18 %, and between 4.3‰ and 5.9‰. C/N_d values range from 10.0 to 17.9. A sharp decrease in $\delta^{13}C_{org}$ and C/N_d values is observed between 5-11 cm which matches positive peaks in TOC, TN_d and $\delta^{15}N_d$ (Fig. 4B). Similar patterns, though less pronounced, are observed at approximately 17 cm, 25 cm, and 40 cm. During onboard sediment slicing, we observed a macroscopic biofilm at a depth of 10 cm having ~~The biofilm is~~ white ~~in~~ color and exhibitings a soft, slimy texture (Fig. S2). ~~(Fig. 5A). The biofilm is white in color and exhibits a soft, slimy texture.~~

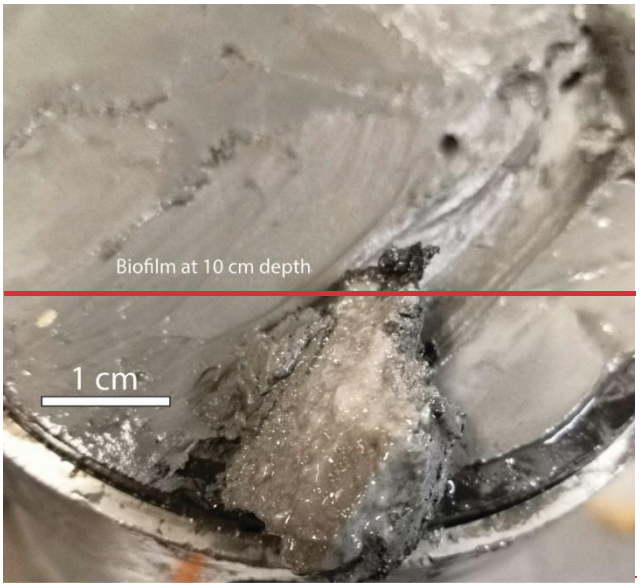

~~**Figure 5. Photograph of a white biofilm encountered at 10 cm while slicing PusC-08. The sediment was sampled every cm in the interval 0-10 cm for microbiological analyses.**~~

4.5 Sediment microbiome

The phylum-level taxonomic composition of 16S rRNA gene–informed ASVs showed a steady, depth-structured shift across the 10-cm sediment column in PusC-08 (Fig. ~~6A~~5A). Triplicates from each depth were largely consistent, with the exception of single outlier replicates at 8 and 9 cm in phylum-level abundances. Across depths, relative abundances changed progressively: Proteobacteria exceeded 50% at 1 cm but declined with depth, such that by 8 cm the community was largely composed of other phyla. In contrast, Desulfobacterota and Campylobacterota increased from the shallow to deeper layers. Around 7 cm, the profile shifted again, with Halobacterota increasing sharply below this horizon. Looking at the same microbial community on a family level (Fig. 5B), the aforementioned depth-structured shift was less apparent and steady. However, notable shifts could be documented. Thioglobaceae decreased over the first 3 cm of depth whereas Sulfurovaeae increased moving down to 7 cm. Below 7 cm of sediment depth, a clear cut in the community structure could be observed after which organisms of the ANME families could be detected.

Alpha- and beta-diversity patterns indicate a depth-structured reorganization of the microbiome across the push-core. Alpha diversity (observed ASVs) rose steadily from 1 to 6 cm, consistent with increasing richness/niche diversification in the upper layers, then declined below 6 cm, coincident with the depth at which the taxonomic profile began to turn over. Beta diversity resolved three depth-associated clusters: a cohesive group comprising all samples from 1–6 cm; a clearly separated group

comprising 8–10 cm; and 7 cm samples positioned between them, consistent with a transitional assemblage. Together, these patterns in PusC-08 point to a stratified microbiome with a boundary around 6–7 cm, above which communities are richer and more similar to one another, and below which communities are less diverse and compositionally distinct.

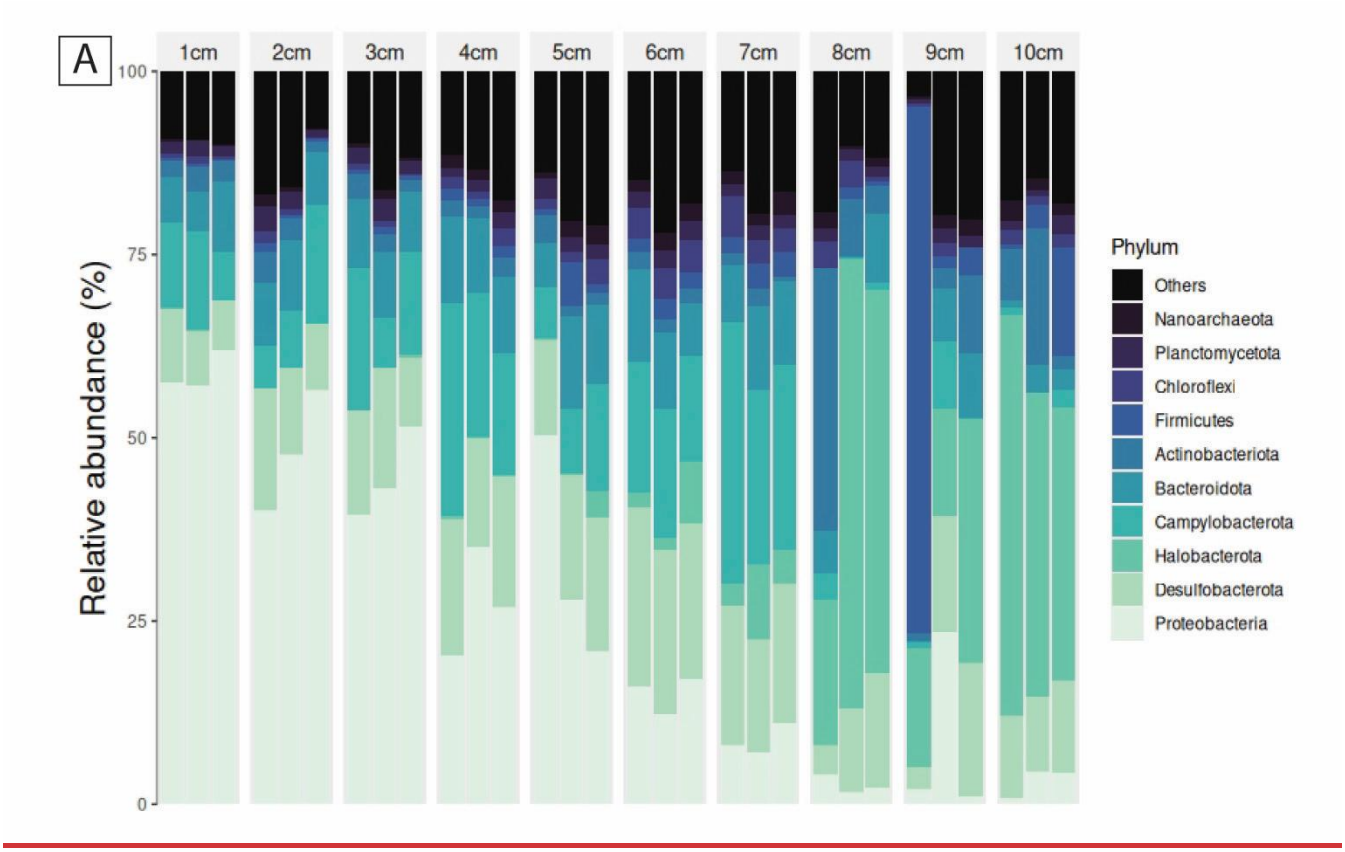
A
1cm
2cm
3cm
4cm
5cm
6cm
7cm
8cm
9cm
10cm
Relative abundance (%)
100
75
50
25
0
Phylum
Others
Nanoarchaeota
Planctomycetota
Chloroflexi
Firmicutes
Actinobacteriota
Bacteroidota
Campylobacterota
Halobacterota
Desulfobacterota
Proteobacteria

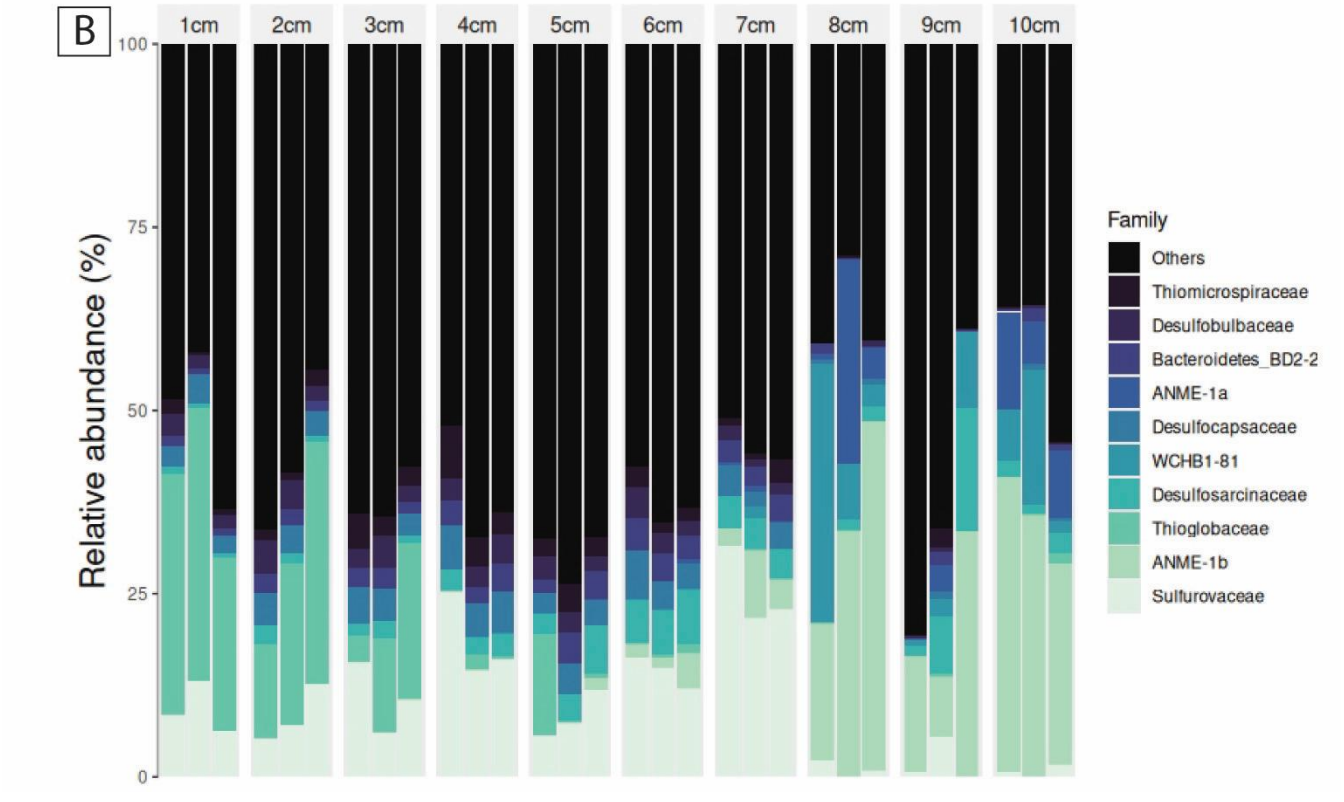
B
1cm
2cm
3cm
4cm
5cm
6cm
7cm
8cm
9cm
10cm
Relative abundance (%)
100
75
50
25
0
Family
Others
Thiomicrospiraceae
Desulfobulbaceae
Bacteroidetes_BD2-2
ANME-1a
Desulfocapsaceae
WCHB1-81
Desulfosarcinaceae
Thioglobaceae
ANME-1b
Sulfurovaceae

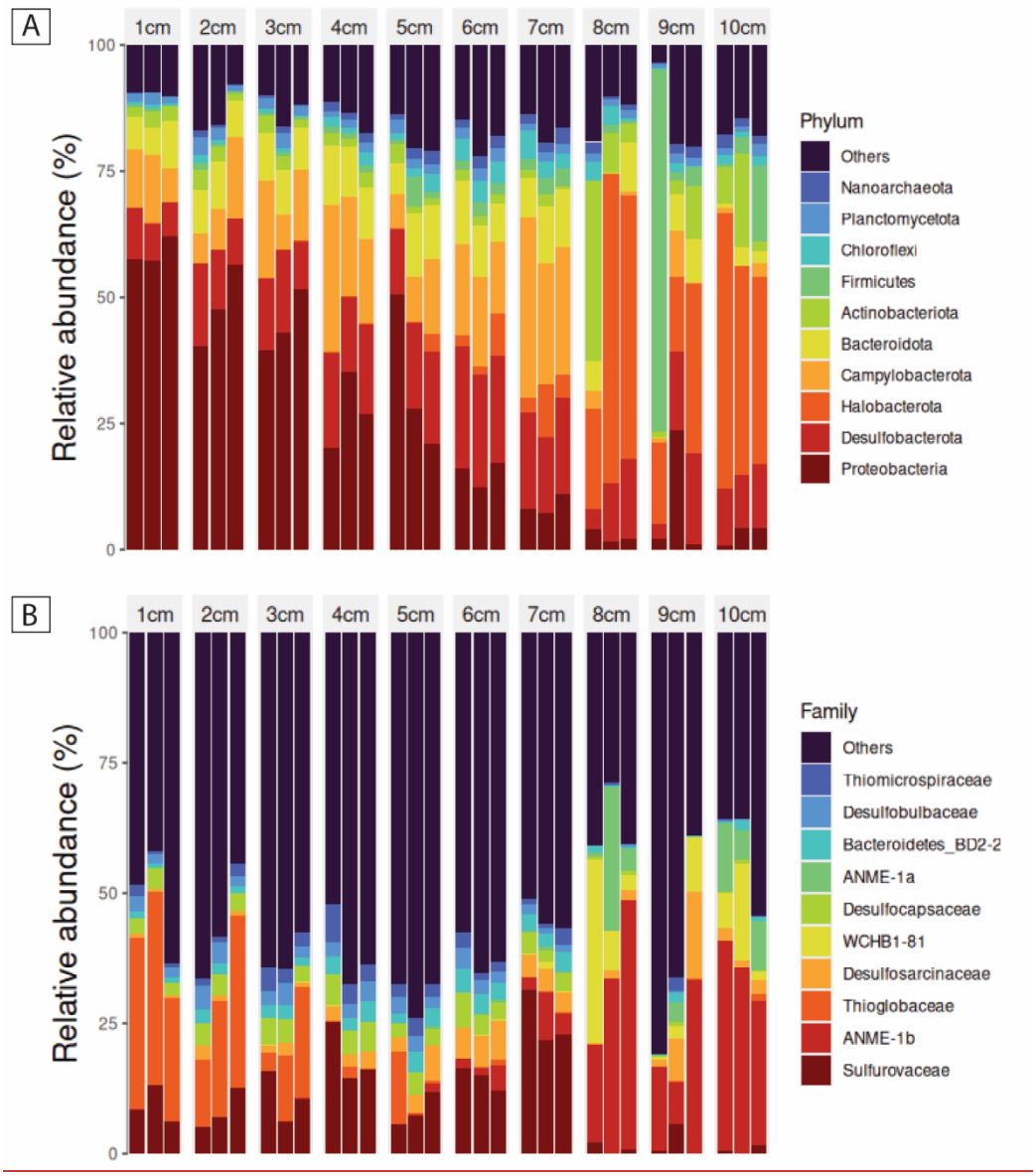

Figure 56. A) Relative abundance of 16S rRNA gene-informed ASVs on phylum level in the first 10 cm of PusC-08. B) Relative abundance of 16S rRNA gene-informed ASVs on family level in the first 10 cm of PusC-08.

5 Discussion

5.1 ~~Biogeochemistry of~~Cold seep biogeochemistry and microhabitats ~~CWC-associated cold seep habitats~~

~~Type and distribution of seafloor habitats in deep marine settings are tightly linked to organic matter fluxes to the sediment surface and remineralization underneath. Organic matter is an important source of nutrients for benthic fauna and microbes, and regulates subsurface biogeochemical processes including methanogenesis (Whiticar, 2020). Within the sediment, microbes break down the organic matter into inorganic substances via a "cascade" of oxidative reactions (respiration) involving different electron acceptors as a function of free energy gain (Schulz and Zabel, 2000; Wehrmann and Ferdelman, 2014). At or near the seafloor, dissolved oxygen (O_2) is energetically more convenient to microbes, whereas moving deeper into the sediments, respiration involves NO_3^-, Mn(IV) and Fe(III) oxides, and SO_4^{2-}, followed by methane formation (Schulz and Zabel, 2000; Whiticar, 2020). These redox processes determine the so called biogeochemical zonation of the sediments which consists of, moving from the seafloor downward, the oxic zone (oxygen reduction zone, aerobic respiration), the suboxic zone (including~~

~~nitrate, manganese and iron reduction zones), and the anoxic zone (including sulfate reduction and methanogenic zones)(Schulz and Zabel, 2000; Tostevin, 2019). The SMTZ is an important redox boundary located between the sulfate reduction zone and the methanogenic zone.~~ Chemosynthetic habitats found at cold seeps rely on hydrogen sulfide fluxes from the SMTZ which are maintained by AOM-sustained sulfate reduction (Foucher et al., 2007; Levin, 2005; Levin et al., 2016~~, p.201~~). There is a causative link between magnitude of methane fluxes, depth of the SMTZ, sulfide fluxes and type of chemosynthetic communities at the seafloor (Argentino et al., 2022b; Fischer et al., 2012; Levin, 2005; Levin et al., 2016; Sahling et al., 2002). Hydrogen sulfide in aquatic environments is generally viewed as a toxicant able to interrupt cellular respiration due to its lipid solubility (Bagarinao, 1992; Riesch et al., 2015; Tobler et al., 2016). Therefore, at cold seeps, only organisms that have adapted to varying levels of sulfide exposure are present and their distribution follows subsurface geochemical gradients. ~~-~~Microbial mats are found in correspondence of the most intense seepage areas with shallower SMTZs (~5-10 cm below the seafloor), whereas higher organisms (clams, mussels, tubeworms) in symbiosis with sulfur-oxidizing bacteria colonize lower-seepage intensity areas ~~with~~ associated with deeper SMTZs (~10-50 cm below the seafloor) (e.g. Fischer *et al.*, 2012; Sen *et al.*, 2018; Lee *et al.*, 2019; Argentino *et al.*, 2022b; Barrenechea *et al.*, 2025). We identified the SMTZs in our cores where a ~~quasi zero~~drop in sulfate content matched a ~~drop~~ decrease in $\delta^{13}C_{DIC}$ and an increase in DIC concentration, evidence of ongoing AOM which consumes sulfate and releases ^{13}C-depleted bicarbonate. ~~Whenever either sulfate or DIC data were absent, we relied on other parameters that were available.~~ In the study area, the SMTZ ranges from ~5 cm (PusC-01, PusC-4) to ~25 cm (PusC-02, PusC-07, PusC-08) (Figs. S1, 3). No SMTZs were intercepted in the other cores. Besides BlaC-01 (and probably gravity core GC-01), all the other cores were collected from microbial mats. However, while the SMTZ depths in PusC-01 and PusC-4 are typical of those expected from microbial mat~~s~~ habitats, the ~~cores outside the mats~~other cores from mats ~~areas~~ showed ~~somewhat anomalous~~deeper SMTZs ~~profiles~~. To interpret the latter case, we considered the morphology and extent of the microhabitats and local biogeochemical and environmental conditions. The high-resolution seafloor imagery and habitat maps show that the sampled mats form small (~~< 50~~~200 cm^2) and highly heterogeneous (shape, color) features with reduced mat thickness giving color shades from white to light grey (Fig. 2). Chemosynthetic mats can rapidly colonize new substrates (e.g. seep sites, vents, wood, whale carcasses) within a few months (Alain et al., 2004; Girard et al., 2020; Guezennec et al., 1998; Kalenitchenko et al., 2016), as well as being rapidly eroded away or consumed by grazers when the chemical substrate is no longer present (Niemann et al., 2013; Seabrook et al., 2019; Sen et al., 2018b; Thurber et al., 2013). The appearance of the mats might therefore suggest that the fluid supply from underneath has been recently decreasing. ~~-~~It is known that cold seeps can be dynamic environments characterized by spatial and temporal variations in gas seepage distribution (Ferré et al., 2020; Greinert, 2008). A substantial variability in seepage activity as seen in water column backscatter anomalies was reported between 2018 and 2022 at this site (Ferré et al., 2024). Temporal fluctuations in methane fluxes ~~is consistent with~~could also explain the concave shape of the sulfate concentration profiles observed in our dataset and deeper SMTZs in some microbial mat microhabitats (Fig. S1). The profile shapes range from concave-up (PusC-04, PusC08?) to concave-down (PusC-07), which is a common indication of rapid increases and decreases in methane flux, respectively (Hensen et al., 2003; Kasten et al., 2003; Minami and Tatsumi, 2012). ~~concave-shaped sulfate profiles in the cores and deeper SMTZs (Kasten et al., 2003). The seep carbonate pavements in the CWC area act as a barrier to upward migrating sulfide-rich fluids, controlling the distribution of mats around the edges of carbonate crusts or in apparently carbonate-free seafloor areas (Fig. 2).~~ Strong bottom currents present in this area (Ferré et al., 2022, 2024) might also contribute to the observed reduced surface area of the single microbial mat patches~~patterns~~, since mats are sensitive to physical disturbances (Cardoso et al., 2019; Noffke, 2010; Pan et al., 2019). Although the ROV samplings were conducted accurately, targeting the inner part of the mat patches, it is possible that the anomalous profiles reflect a mixed signal due to the sampling area of our coring devices (push corer = 50 cm²; blade corer = 250 cm²) being comparable to the size of the investigated microhabitats. Moreover, the ex-situ pore water extraction using 5-cm long rhizon filters inserted transversally into the core stratigraphy is also yielding bulk geochemical values. In-situ sensors such as the Raman probe (Zhang et al., 2010, 2011), are crucial for

resolving challenges associated with cm-scale horizontal variations in geochemical gradients in microhabitats of small extent, such as those mapped in our study. ~~(Zhang et al., 2010, 2011)~~Regarding the spatial distribution of microhabitats, t~~T~~he seep carbonate pavements in the CWC area act as a barrier to upward migrating sulfide-rich fluids, controlling the distribution of mats around the edges of carbonate crusts or in apparently carbonate-free seafloor areas (Fig. 2). Siboglinid tubeworms are common at Arctic cold seeps (Argentino et al., 2022b; Sen et al., 2018b, a) and represent the dominant benthic community at nearby seeps in canyons on the lower continental slope off Lofoten–Vesterålen islands (Sen et al., 2019). The general lack of tubeworms in the investigated seepage site must be related to the sedimentary substrate (Bellec et al., 2024; Sen et al., 2019), i.e. hard carbonate pavements and/or coarse sediment (Fig. 2), since tubeworms require softer sediments to settle (Hilário et al., 2011; Southward et al., 2005).

Geochemical anomalies in $\delta^{13}C$ of foraminifera in PusC08 appear below ~20 cm, with remarkably negative isotopic values. This data reflects ongoing or past precipitation of methane-derived carbonate as secondary overgrowth on the tests and it is widely used in paleo-seep reconstructions (Argentino et al., 2021, 2024; Boretto et al., 2026; Schneider et al., 2018; Yao et al., 2020). In PusC-08 these anomalies match the modern SMTZ as indicated by DIC data and the sharp drop in sulfate concentration right above (Fig. 4). Based on these observations, we ascribe the foraminiferal anomalies to MDAC formation at the modern SMTZ.

~~Overall, our multidisciplinary dataset demonstrates that the combination of a methane-charged sediment and a high-energy oceanographic setting favoring steady food supply are prerequisites for CWC development in this area. Moreover, microbial mats and MDACs were frequently observed in direct contact with CWCs (either adjacent to or at their base) during ROV dives (Ferré et al., 2024), although in our orthomosaics and habitat maps (Fig. 2) corals are absent. The CWCs in this area are always associated with chemosynthetic substrates and bubbling, but not vice versa. This suggests that seafloor emissions alone do not play a key role in controlling coral distribution, as they show neither strong positive nor negative effects. Instead, CWCs appear to selectively grow on outcropping hard substrates located at local seafloor topographic reliefs (Ferré et al., 2024).~~

5.2 Geochemical and genetic indications of methanotrophic biomass within the sediments

In this section we interpret the geochemical anomalies measured in the sediment of PusC-08 and discuss the putative origin of ~~the~~ a white biofilm found at 10 cm ~~below the seafloor~~in the same core (Fig. S2)~~(Fig. 5)~~. Generally, the bulk organic matter composition of marine sediments includes a mixture of marine algae and vascular plants debris from land (Burdige, 2005; Emerson and Hedges, 1988; Meyers, 1994, 1997). The elemental and isotopic signatures of these two categories have been widely used for assessing the contribution of marine versus terrestrial organic inputs in paleoceanography (e.g. Kang *et al.*, 2007; Knies & Martinez, 2009; Hasegawa *et al.*, 2013; Knies, 2022). Marine-derived organic matter is commonly associated with $\delta^{13}C$ values between −23‰ and − 16‰ (Emerson and Hedges, 1988; Meyers, 1994), $\delta^{15}N$ values as high as 7‰ (Wada, 1980), and C/N ratios between 4 and 10 (Meyers, 1994). Terrestrial organic matter from C3 plants which dominate the Arctic regions has lower $\delta^{13}C$ values < −25‰ (Meyers, 1994; Naidu et al., 2000; Rachold and Hubberten, 1999; Ruttenberg and Goñi, 1997), $\delta^{15}N$ values ~0‰ (Kienast et al., 2005), and C/N ratios > 20 (Emerson and Hedges, 1988; Meyers, 1994). These ranges can vary regionally but they hold true for most marine settings, with minor adjustments of the end-member compositions (Argentino et al., 2023; Knies et al., 2007; Knies and Martinez, 2009). In PusC-08, $\delta^{13}C_{org}$ reaches values as negative as −43.4‰, which cannot be explained by a simple mixture of marine and terrestrial organic matter. Similar values in bulk sediment were reported from cold seeps in the SW Barents Sea (−42‰, Argentino *et al.*, 2023b), offshore Pakistan (−42‰, Yoshinaga *et al.*, 2014) and interpreted as indicative of significant contributions of methanotrophic biomass to the organic matter pool. In fact, methanotrophic microbes inhabiting cold seeps incorporate variable amounts of isotopically-fractionated carbon from methane (Kurth et al., 2019; Stock et al., 2025; Wegener et al., 2008), which is known to carry negative $\delta^{13}C$ signals, generally < −50‰ (Judd and Hovland, 2007; Milkov and Etiope, 2018; Whiticar, 2020). Therefore, we confidently

ascribe the isotopically-depleted $\delta^{13}C$ values in PusC-08 between 5.5 cm and 11.5 cm to higher contents of methanotrophic biomass. The concomitant drop in C/N_d values in that interval supports this interpretation, since bacterial organic matter has low C/N ratios ~5 (Madigan et al., 2017). Differently from other studies reporting a decrease in $\delta^{15}N$ in AOM-impacted layers (Argentino et al., 2023; Hu et al., 2020), here we observe a slight increase (Fig. 4). This difference can be due to different nitrogen assimilation pathways by AOM-SRB consortia and/or different nitrogen substrates isotopic composition (Dekas et al., 2009, 2014; Gruber and Galloway, 2008). This AOM-impacted interval hosts a biofilm and is stratigraphically located above the modern SMTZ (Fig. 4). Macroscopic biofilms similar to the one found in our study have been reported by Briggs et al. (2011) from methane seeps at Hydrate Ridge (offshore of Oregon, USA), northern Cascadia Margin (offshore of Vancouver Island, Canada), and the Indian Ocean (offshore India), and by Gründger et al. (2019) from gas hydrate pingoes in the NW Barents Sea. In those studies, the biofilms consist of ANME-SRB consortia performing AOM (Briggs et al., 2011; Gründger et al., 2019), and the reported isotopic values for the pure biofilm masses yielded $\delta^{13}C$ as negative as −43‰ (Briggs et al., 2011). We did not conduct carbon-nitrogen analyses on the biofilm material to directly compare with previous studies, but we found a similar value (−43.4‰) in bulk sediment from the same interval. What leads to the accumulation of macroscopic masses is the occurrence of pockets, cracks or fractures within the sediment, which provide high accommodation space (Briggs et al., 2011; Gründger et al., 2019). In PusC-08 we observed a network of microfractures in the core but no clear correlation with biofilm position was noticed during sediment slicing. The lack of indication of paleo-SMTZs in geochemical profiles of foraminifera (Fig. 4B) enable us to exclude that the biofilm could represent past conditions with higher methane fluxes but rather suggests ongoing activity. The stratigraphic position of the biofilm suggests that there is methane bypassing the SMTZ and being locally consumed within fractures (Briggs et al., 2011).

~~We extrapolated the isotopic ($\delta^{13}C_{org}$, $\delta^{15}N_d$) and elemental (atomic C/N) compositions of the methanotrophic end-member via modeling of the respective downcore profiles. We selected the interval 5.5–10.5 cm which hosts steep linear isotopic gradients which we hypothesize to indicate the presence of AOM-related biomass. The slope of the linear fit to the plot $\delta^{13}C_{org}$ x TOC to TOC values (Fig. 7A) provides the $\delta^{13}C_{org}$ composition of the TOC added to the sediment (Coffin et al., 2017) which generates the anomaly seen in the profile. Our model yielded $\delta^{13}C_{org}$ = −73.7‰ (r^2 = 0.96; n =6). This value agrees well with previous studies on methane seep microbiota (House et al., 2009) and with $\delta^{13}C_{org}$ values as negative as −81‰ measured on methanotrophic-dominated biomass contained in methane-derived carbonates (Feng et al., 2021). The same modeling approach was applied to $\delta^{15}N_d$ (plot $\delta^{15}N_d$ x TN_d to TN_d) and the resulting $\delta^{15}N_d$ value is 6.9‰ (r^2 = 0.99; n =6) (Fig. 7B). (Argentino et al., 2023; Hu et al., 2020)Argentino *et al.* (2023) found much lower isotopic values in methanotrophic-influenced sediments from Håkon Mosby Mud Volcano. This difference can be interpreted as due to different nitrogen assimilation pathways by AOM-SRB consortia and/or different nitrogen substrates isotopic composition (Dekas et al., 2009, 2014; Gruber and Galloway, 2008). For the calculation of the atomic C/N ratio, we normalized TOC and TN_d by their atomic weights of 12.011 and 14.007, respectively, and plotted their normalized values TN_d to TOC (Fig. 7C). The linear regression equation (TN_d = 0.1399 x TOC − 0.008) was used to calculate the TOC value when the TN_d = 1. The resulting value of 7.2 is consistent (within uncertainties of the model) with a microbial end-member (Madigan et al., 2017). We did not conduct carbon-nitrogen analysis on pure biofilm material found at 10 cm but the good fit of the regression models of sediment samples which include the biofilm points to a unique end-member. The biofilm would represent microbial consortia performing AOM which are spread over the 5.5–11.5 cm interval and locally accumulated at 10 cm to form a macroscopic feature.~~

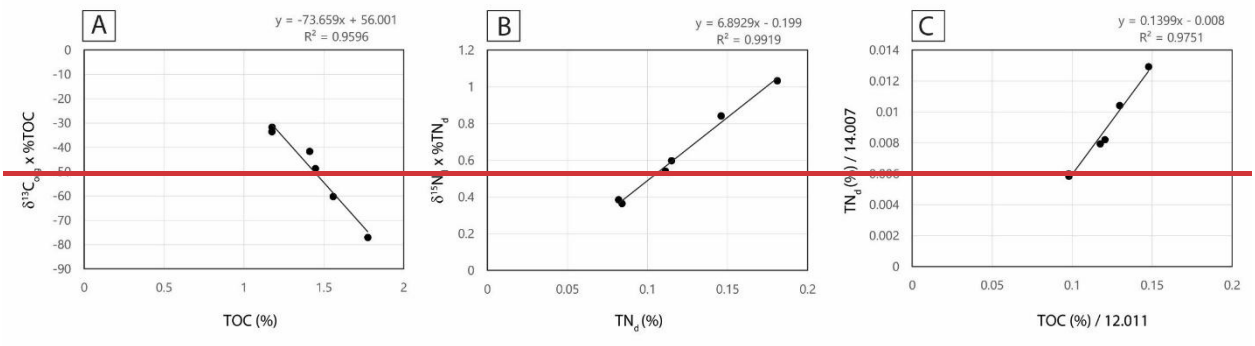

~~Figure 7. Linear regression models used for the extrapolation of the methanotrophic end-member in the sediment interval 5.5-11.5 cm of PusC.08. A) Plot of measured $\delta^{13}C_{org}$ x TOC concentrations vs. TOC (%); B) Plot of measured $\delta^{15}N_d$ x TN_d concentrations vs. TN_d (%); C) Plot of TN_d vs TOC concentrations normalized for their atomic masses. The slopes of the linear fits are presented in the equation above each plots.~~

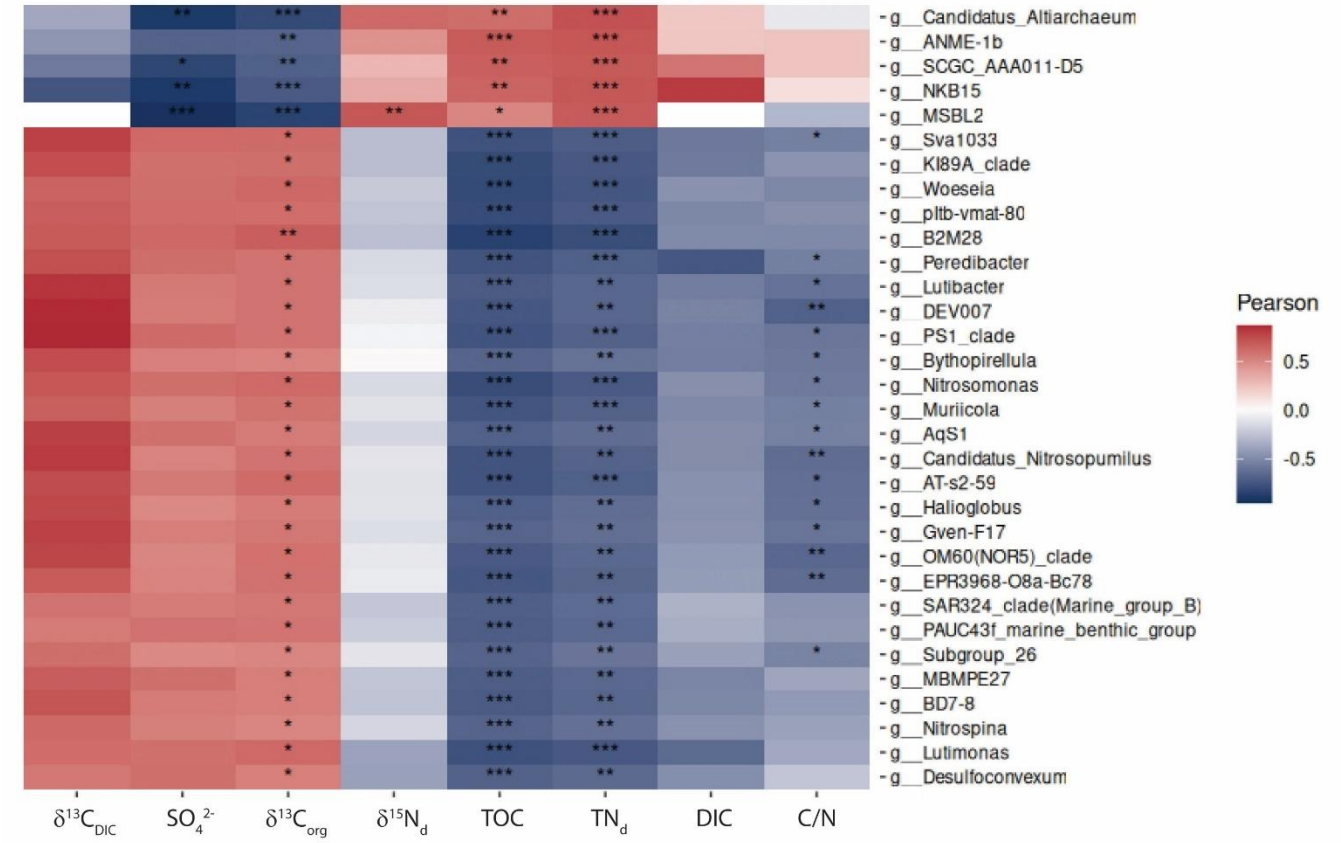

Figure ~~8~~6. Pearson correlation of environmental parameters and 16S rRNA gene-informed ASVs on genus level. Only genera with at least one high score "***" correlation were selected.

~~Future metagenomic analyses will be conducted on samples from PusC-08 for identifying the key microbial players and their ecological roles.~~ CStill, correlations between biogeochemical parameters from pore waters and carbon-nitrogen ~~s~~geochemistry with 16S rRNA ASVs at the genus level reveal a clear division of the microbial community into two distinct groups, driven primarily by TOC, TN_d, SO_4^{2-}, and $\delta^{13}C_{org}$ (Fig. ~~6~~8). The first group, comprising archaeal taxa, is associated with organic-rich, nitrogen-rich, sulfate-depleted environments and plays a key role in methane oxidation and carbon fixation. In contrast, the second group, consisting largely of bacterial taxa, thrives in sulfate-rich, inorganic carbon-enriched conditions and is involved in sulfate reduction and sulfur cycling, highlighting the complementary roles of these groups in driving key biogeochemical processes.

The first group includes the top 5 genera: g__Candidatus_Altiarchaeum, g__ANME-1b, g__SCGC_AAA011-D5, g__MSBL2, and g__NKB15. Among these, g__Candidatus_Altiarchaeum is known to act as a carbon dioxide sink, contributing to carbon fixation(Probst et al., 2014). Similarly, g__SCGC_AAA011-D5 belongs to the Nanoarchaeota archaeon, which is also adapted to anaerobic conditions. g__MSBL2 (classified as Methylocella) is a methanotroph, suggesting its involvement in methane oxidation. Together, these taxa likely contribute to carbon fixation, methane cycling, and organic matter degradation. The negative correlation with $\delta^{13}C_{org}$ suggests that these taxa, particularly g__ANME-1b, use isotopically light organic matter, likely incorporating the strongly negative isotopic signature of methane-derived carbon into their biomass, further supporting their potential link to anaerobic methane oxidation (AOM). The second group is more diverse, with many taxa positively correlated with SO_4^{2-} and $\delta^{13}C_{org}$, suggesting adaptation to sulfate-rich environments and involvement in sulfur cycling, likely including sulfate-reducing bacteria (SRB). Other genera showing strong inverse correlations with sulfate concentration in pore water and with $\delta^{13}C_{org}$ correspond to sulfate-reducing *Deltaproteobacteria* which assimilates bicarbonate released by organoclastic sulfate reduction in marine sediments, i.e. MSBL2 (Vuillemin et al., 2022). The positive correlation with $\delta^{13}C$ ~~indicates a~~could indicate preference for isotopically heavier carbon sources, potentially linked to sulfur-based metabolic pathways. Other correlations relate to genera which are found in "normal" marine sediments unaffected by seepage. Future metagenomic analyses will be conducted on samples from PusC-08 for identifying the key microbial players and their ecological roles.

~~Macroscopic biofilms similar to the one found in our study have been reported by Briggs et al. (2011) from methane seeps at Hydrate Ridge (offshore of Oregon, USA), northern Cascadia Margin (offshore of Vancouver Island, Canada), and the Indian Ocean (offshore India), and by Gründger et al. (2019) from gas hydrate pingoes in the NW Barents Sea. In those studies, the biofilms consist of ANME-SRB consortia performing AOM (Briggs et al., 2011; Gründger et al., 2019), and the reported isotopic values for the pure biofilm masses yielded $\delta^{13}C$ as negative as −43‰ (Briggs et al., 2011). We speculate that in our case the modelled biofilm isotopic composition has lighter $\delta^{13}C$ due to relatively larger incorporation of methane-derived carbon (Kurth et al., 2019; Wegener et al., 2008). These biofilms, including the one in our study, are always associated with shallow SMTZs at cold seeps. What leads to the accumulation of macroscopic masses is the occurrence of pockets, cracks or fractures within the sediment, which provide high accommodation space (Briggs et al., 2011; Gründger et al., 2019). In PusC-08 we observed a network of microfractures in the core but no clear correlation with biofilm position was noticed during sediment slicing. The biofilm is located slightly above the SMTZ zone defined using pore water profiles (Fig. 3), which suggests that there is methane bypassing the SMTZ and being locally consumed within fractures (Briggs et al., 2011). The lack of indication of paleo-SMTZs in geochemical profiles of foraminifera (Fig. 4B) enable us to exclude that the biofilm could represent past conditions with higher methane fluxes, but rather suggests ongoing activity. In summary, cold seeps offshore Vesterålen islands revealed a unique Arctic environment where CWCs coexist with seafloor chemosynthetic communities and local sedimentary hotspots of methane oxidation.~~

5.3 Geomorphological and biogeochemical factors influencing the distribution of CWCs at the Vesterålen site

Along the Norwegian coast, several coral fields have been mapped over the last decades by MAREANO (www.mareano.no; ~~(~~Hovland, 2008b), with some reef associations with hydrocarbon seeps. Among them, the Hola Trough became a case study to investigate the relationships between corals and seeps and monitor their response to environmental perturbations such as ocean acidification. Our study is part of a larger set of investigations conducted within the EMAN7 project. Here we did not focus the analyses on corals, but on the cold seep environment over which they superimpose. Still, we can discuss our results in light of recently-published studies from EMAN7 (Ferré et al., 2024; Sert et al., 2025), and previous work in the same area (e.g. Crémière et al., 2016; Hovland, 1990; Hovland and Thomsen, 1997; Sauer et al., 2015, 2017), to draw some lines of evidence about the geological and biogeochemical influence of seeps on CWCs. During ROV Dives conducted in 2022 (Ferré

et al., 2022) microbial mats and MDACs were frequently observed in direct contact (either adjacent to or at their base) with coral mounds shown in Fig. 1b (Ferré et al., 2024), although in our orthomosaics and habitat maps covering the broader seepage environment (Fig. 2) corals are absent. Based on ROV imagery and the generated datasets, we found that CWCs in this area are mostly associated with chemosynthetic substrates (MDAC, microbial mats) and bubbling (Ferré et al., 2024). This is true also for the site to the north-east of the three mosaics, where hundreds of corals occur inside an intense gas emission area (Ferré et al., 2024). From a sediment perspective, we do not expect any difference in methane-related biogeochemical processes getting closer or further from CWCs, with AOM-associated sulfide fluxes sustaining chemosynthesis at the seafloor in spots where the MDAC "seal" is broken. Sub-bottom profiles crossing the two main mounds and reported in (Ferré et al., 2024) revealed that the CWCs occur on top of topographic highs, likely related to glacial deposits (Buhl-Mortensen et al., 2012), which overly gas accumulations. Gas seeps identified outside of the profile coverage also show a correlation with small positive structures in the seafloor morphology. Our microbathymetric maps revealed a relatively flat morphology dominated by carbonate pavements. There is a strong topographic control for both gas migration in the shallow subsurface and coral occurrence. The presence of widespread MDAC deposits close to or at the seafloor explains the gas migration paths, which concentrate the gas toward topographic highs. Long-lasting seepage of deep-sourced thermogenic gas (Crémière et al., 2016; Sauer et al., 2015, 2017) resulted in the formation of widespread hard substrate, while the elevated structures shaped by glacial activity provided better exposure to strong bottom currents that supply food to the corals. At the CWC mounds, cold seeps influence the chemical and isotopic composition of dissolved organic carbon (Sert et al., 2025). Whether there is any seep-derived carbon uptake from corals remains unclear~~(Sert et al., 2025)~~. Future results from ongoing coral transplantation experiments at this site will offer insights into this and other biochemical processes.

~~Overall, our multidisciplinary dataset demonstrates that the combination of a methane-charged sediment and a high-energy oceanographic setting favoring steady food supply are prerequisites for CWC development in this area. Moreover, microbial mats and MDACs were frequently observed in direct contact with CWCs (either adjacent to or at their base) during ROV dives (Ferré et al., 2024), although in our orthomosaics and habitat maps (Fig. 2) corals are absent. The CWCs in this area are always associated with chemosynthetic substrates and bubbling, but not vice versa. This suggests that seafloor emissions alone do not play a key role in controlling coral distribution, as they show neither strong positive nor negative effects. Instead, CWCs appear to selectively grow on outcropping hard substrates located at local seafloor topographic reliefs (Ferré et al., 2024).~~

6 Conclusions

Methane seepage in the Hola area off the coast of Vesterålen (northern Norway) is known for its peculiar association with *Desmophyllum pertusum* cold water corals, but only recently it was possible to explore the distribution of seafloor ecosystems and to conduct microhabitat-specific samplings for biogeochemical investigations. Using ROV imagery collected in 2022 during expedition CAGE22-3, we generated three orthomosaics at millimetric resolution and habitat maps covering a total area of 1,307 m² in proximity of two coral mounds. ~~and habit maps for three smaller areas in proximity to the coral mounds.~~ A striking feature of this site is the presence of widespread MDAC pavements, partially exposed at the seafloor. White microbial mats forming small patches with an average area of 200 cm^2 ~~(a few tens of cm)~~ thrive along the edges of exposed carbonate crusts and on ~~their fractures~~sedimented spots. We discussed the peculiar morphology and extent of mat microhabitats at this site, which are influenced by seep-related and environmental factors: widespread carbonate cap that channels rising fluids, spatial and temporal variations in methane flux, and strong bottom currents. –We ~~collected~~ report the pore fluid composition of ~~9~~nine ROV-guided pushcores and blade cores from mats ~~(whenever sediment cover permitted)~~ and background areas to compare their subsurface biogeochemistry and link it to seafloor habitats~~observations~~. Sulfate-methane transition

zones as shallow as ~5 cm and an increase in DIC carrying a ^{13}C-depleted methane signature are measured beneath the mats, indicating high methane fluxes and intense AOM ~~rates~~. Pore water profiles show concave-up and concave-down shapes, which reflect temporal variations in methane flux in agreement with variable seepage activity observed in cruises in the same area. ~~A pushcore from a mat revealed the presence of a buried macroscopic white biofilm at 10 cm.~~ Organic matter (TOC, $\delta^{13}C$, TN_d, $\delta^{15}N$) and 16S rRNA gene analyses on this core provide evidence for the accumulation of methanotrophic biomass leading to bulk sediment $\delta^{13}C_{org}$ values as negative as −43.4‰ and putatively attributed to ANME-1b anaerobic methane-oxidizing archaea. ~~dominated by ANME anaerobic methane oxidizing archaea leading to bulk sediment $\delta^{13}C$ values as negative as −43.4‰. Secondary overgrowth of MDAC on foraminiferal tests was identified by bulk $\delta^{13}C$ values as low as − 18.5‰. These anomalies match the modern SMTZ interval with pore waters showing the highest DIC concentration and lightest DIC isotopic composition ($\delta^{13}C$ = −29.8‰), thus suggesting ongoing carbonate precipitation.~~ The same AOM-impacted interval hosts ~~A pushcore from a mat revealed the presence of a buried~~a macroscopic white biofilm ~~at 10 cm~~located above the modern SMTZ that will be characterized in future studies. ~~.~~

~~Corals in this area are spatially linked to chemosynthetic substrates and bubbling, though the reverse is not true, indicating that seafloor emissions do not influence directly the local coral distribution. Nonetheless, the presence of seep-related carbonate outcrops and high energy currents (major suppliers of food source for CWCs), remains the strongest prerequisite for the development of cold-water corals, which in this specific area seem to settle preferentially on elevated seafloor reliefs.~~

Data availability

Microbathymetry and orthomosaics from the EMAN7 Expedition 2022 are openly available on Dataverse.NO at https://doi.org/10.18710/1FCVAE. Geochemistry data are currently accessible to reviewers during the review process and will be made publicly available upon publication. Raw sequencing DNA data have been submitted to the European Nucleotide Archive (ENA) and will be available under accession PRJEB96327.

Author contributions

G.P. and C.A. conceived the study and conducted the sediment and pore fluid samplings onboard, C.A. wrote the initial manuscript with specific inputs from S.B., H.C.B and I.B. for the microbiological section, J.G.C. for the introduction on corals, and L.F. for image processing. C.A., L.F. and S.B. produced the figures and tables. All the authors contributed to the discussion and improvement of the paper since the early draft.

Competing interests

The authors declare that they have no conflict of interest.

Acknowledgments

This research was funded by EMAN7 project (Research Council of Norway grant No. 320100) and supported by AKMA project (Research Council of Norway grant No. 287869) and EXTREMES (UArctic UA 06/2024). We acknowledge the captain and crew onboard R/V Kronprins Hakon for their assistance during the expedition. We are grateful to Abidemi Akinselure and Matteus Lindgren (SIL-UiT) for sample preparation and IRMS analyses. Publication costs are covered by UiT's Publishing Fund. We thank the two anonymous reviewers and associate editor Mark Lever for constructive feedback.

References

Aalto, N. J., Schweitzer, H. D., Krsmanovic, S., Campbell, K., and Bernstein, H. C.: Diversity and Selection of Surface Marine Microbiomes in the Atlantic-Influenced Arctic, Front. Microbiol., 13, 892634, https://doi.org/10.3389/fmicb.2022.892634, 2022.

Alain, K., Zbinden, M., Le Bris, N., Lesongeur, F., Quérellou, J., Gaill, F., and Cambon-Bonavita, M.: Early steps in microbial colonization processes at deep-sea hydrothermal vents, Environ. Microbiol., 6, 227–241, https://doi.org/10.1111/j.1462-2920.2003.00557.x, 2004.

Argentino, C., Conti, S., Crutchley, G. J., Fioroni, C., Fontana, D., and Johnson, J. E.: Methane-derived authigenic carbonates on accretionary ridges: Miocene case studies in the northern Apennines (Italy) compared with modern submarine counterparts, Mar. Pet. Geol., 102, 860–872, https://doi.org/10.1016/j.marpetgeo.2019.01.026, 2019.

Argentino, C., Waghorn, K. A., Vadakkepuliyambatta, S., Polteau, S., Bünz, S., and Panieri, G.: Dynamic and history of methane seepage in the SW Barents Sea: new insights from Leirdjupet Fault Complex, Sci. Rep., 11, 4373, https://doi.org/10.1038/s41598-021-83542-0, 2021.

Argentino, C., Lee, A., Fallati, L., Sahy, D., Birgel, D., Peckmann, J., Bünz, S., and Panieri, G.: Biogeochemistry and timing of methane-derived carbonate formation at Leirdjupet fault complex, SW Barents sea, Front. Earth Sci., 10, 1–23, https://doi.org/10.3389/feart.2022.1029471, 2022a.

Argentino, C., Savini, A., and Panieri, G.: Integrating Fine-Scale Habitat Mapping and Pore Water Analysis in Cold Seep Research: A Case Study from the SW Barents Sea, in: World Atlas of Submarine Gas Hydrates in Continental Margins, Springer International Publishing, Cham, 505–514, https://doi.org/10.1007/978-3-030-81186-0_43, 2022b.

Argentino, C., Wittig, C., Peckmann, J., and Panieri, G.: Nitrogen uptake by methanotrophic consortia in deep-water gas hydrate-bearing sediments, Chem. Geol., 636, 121638, https://doi.org/10.1016/j.chemgeo.2023.121638, 2023.

Argentino, C., Borrelli, C., Akinselure, A., Correa-Diaz, M., and Panieri, G.: Biogeochemical investigations of methane seepage at the ultraslow-spreading Arctic mid-ocean ridge: Svyatogor ridge, Fram Strait, Mar. Pet. Geol., 162, 106761, https://doi.org/10.1016/j.marpetgeo.2024.106761, 2024.

Bagarinao, T.: Sulfide as an environmental factor and toxicant: tolerance and adaptations in aquatic organisms, Aquat. Toxicol., https://doi.org/10.1016/0166-445X(92)90015-F, 1992.

Barrenechea, I. A., Argentino, C., Cermakova, K., Holzmann, M., Pawlowski, J., and Panieri, G.: Sediment eDNA metabarcoding reveals the endemism in benthic foraminifera from Arctic methane cold seepages, ISME Commun., ycaf058, https://doi.org/10.1093/ismeco/ycaf058, 2025.

Beaumont, N. J., Austen, M. C., Atkins, J. P., Burdon, D., Degraer, S., Dentinho, T. P., Derous, S., Holm, P., Horton, T., Van Ierland, E., Marboe, A. H., Starkey, D. J., Townsend, M., and Zarzycki, T.: Identification, definition and quantification of goods and services provided by marine biodiversity: Implications for the ecosystem approach, Mar. Pollut. Bull., 54, 253–265, https://doi.org/10.1016/j.marpolbul.2006.12.003, 2007.

Becker, E. L., Cordes, E. E., Macko, S. A., and Fisher, C. R.: Importance of seep primary production to Lophelia pertusa and associated fauna in the Gulf of Mexico, Deep Sea Res. Part Oceanogr. Res. Pap., 56, 786–800, https://doi.org/10.1016/j.dsr.2008.12.006, 2009.

Bellec, V. K., Chand, S., Knies, J., Bjarnadóttir, L. R., Lepland, A., Sen, A., and Thorsnes, T.: New cold seep sites on the continental slope southwest to Svalbard, Front. Earth Sci., 12, 1328357, https://doi.org/10.3389/feart.2024.1328357, 2024.

Benz, U. C., Hofmann, P., Willhauck, G., Lingenfelder, I., and Heynen, M.: Multi-resolution, object-oriented fuzzy analysis of remote sensing data for GIS-ready information, ISPRS J. Photogramm. Remote Sens., 58, 239–258, https://doi.org/10.1016/j.isprsjprs.2003.10.002, 2004.

Biastoch, A., Treude, T., Rpke, L. H., Riebesell, U., Roth, C., Burwicz, E. B., Park, W., Latif, M., Böning, C. W., Madec, G., and Wallmann, K.: Rising Arctic Ocean temperatures cause gas hydrate destabilization and ocean acidification, Geophys. Res. Lett., 38, 1–6, https://doi.org/10.1029/2011GL047222, 2011.

Blaschke, T.: Object based image analysis for remote sensing, ISPRS J. Photogramm. Remote Sens., 65, 2–16, https://doi.org/10.1016/j.isprsjprs.2009.06.004, 2010.

Blumenberg, M., Walliser, E.-O., Taviani, M., Seifert, R., and Reitner, J.: Authigenic carbonate formation and its impact on the biomarker inventory at hydrocarbon seeps – A case study from the Holocene Black Sea and the Plio-Pleistocene Northern Apennines (Italy), Mar. Pet. Geol., 66, 532–541, https://doi.org/10.1016/j.marpetgeo.2015.05.013, 2015.

Bøe, R., Bellec, V. K., Dolan, M. F. J., Buhl-Mortensen, P., Rise, L., and Buhl-Mortensen, L.: Cold-water coral reefs in the Hola glacial trough off Vesterålen, North Norway, Geol. Soc. Lond. Mem., 46, 309–310, https://doi.org/10.1144/M46.8, 2016.

Boetius, a, Ravenschlag, K., Schubert, C. J., Rickert, D., Widdel, F., Gieseke, a, Amann, R., Jørgensen, B. B., Witte, U., and Pfannkuche, O.: A marine microbial consortium apparently mediating anaerobic oxidation of methane., Nature, 407, 623–626, https://doi.org/10.1038/35036572, 2000.

Boetius, A. and Wenzhöfer, F.: Seafloor oxygen consumption fuelled by methane from cold seeps, Nat. Geosci., 6, 725–734, https://doi.org/10.1038/ngeo1926, 2013.

Boretto, G. M., Sabino, M., Torricella, F., Ingrosso, G., Nogarotto, A., Panieri, G., Hefter, J., Mollenhauer, G., Langone, L., Giuliani, S., Tesi, T., and Capotondi, L.: Taphonomic signature of benthic foraminifera linked to methane release in the Barents Sea, Mar. Geol., 492, 107693, https://doi.org/10.1016/j.margeo.2025.107693, 2026.

Briggs, B. R., Pohlman, J. W., Torres, M., Riedel, M., Brodie, E. L., and Colwell, F. S.: Macroscopic Biofilms in Fracture-Dominated Sediment That Anaerobically Oxidize Methane, Appl. Environ. Microbiol., 77, 6780–6787, https://doi.org/10.1128/AEM.00288-11, 2011.

Buhl-Mortensen, L., Bøe, R., Dolan, M. F. J., Buhl-Mortensen, P., Thorsnes, T., Elvenes, S., and Hodnesdal, H.: Banks, Troughs, and Canyons on the Continental Margin off Lofoten, Vesterålen, and Troms, Norway, in: Seafloor Geomorphology as Benthic Habitat, Elsevier, 703–715, https://doi.org/10.1016/B978-0-12-385140-6.00051-7, 2012.

Burdige, D. J.: Burial of terrestrial organic matter in marine sediments: A re-assessment, Glob. Biogeochem. Cycles, 19, https://doi.org/10.1029/2004GB002368, 2005.

Callahan, B. J., McMurdie, P. J., Rosen, M. J., Han, A. W., Johnson, A. J. A., and Holmes, S. P.: DADA2: High-resolution sample inference from Illumina amplicon data, Nat. Methods, 13, 581–583, https://doi.org/10.1038/nmeth.3869, 2016.

Cardoso, D. C., Cretoiu, M. S., Stal, L. J., and Bolhuis, H.: Seasonal development of a coastal microbial mat, Sci. Rep., 9, 9035, https://doi.org/10.1038/s41598-019-45490-8, 2019.

Chand, S., Rise, L., Bellec, V., Dolan, M., Bøe, R., Thorsnes, T., and Buhl-Mortensen, P.: Active Venting System Offshore Northern Norway, Eos Trans. Am. Geophys. Union, 89, 261–262, https://doi.org/10.1029/2008EO290001, 2008.

Crémière, A., Lepland, A., Chand, S., Sahy, D., Condon, D. J., Noble, S. R., Martma, T., Thorsnes, T., Sauer, S., and Brunstad, H.: Timescales of methane seepage on the Norwegian margin following collapse of the Scandinavian Ice Sheet, Nat. Commun., 7, 11509, https://doi.org/10.1038/ncomms11509, 2016.

Dekas, A. E., Poretsky, R. S., and Orphan, V. J.: Deep-Sea Archaea Fix and Share Nitrogen in Methane-Consuming Microbial Consortia, Science, 326, 422–426, https://doi.org/10.1126/science.1178223, 2009.

Dekas, A. E., Chadwick, G. L., Bowles, M. W., Joye, S. B., and Orphan, V. J.: Spatial distribution of nitrogen fixation in methane seep sediment and the role of the ANME archaea, Environ. Microbiol., 16, 3012–3029, https://doi.org/10.1111/1462-2920.12247, 2014.

Deng, Y., Chen, F., Li, N., Jin, M., Cao, J., Chen, H., Zhou, Y., Wu, C., Zhuang, C., Zhao, Y., and Cheng, S.: Cold-Water Corals in Gas Hydrate Drilling Cores from the South China Sea: Occurrences, Geochemical Characteristics and Their Relationship to Methane Seepages, Minerals, 9, 742, https://doi.org/10.3390/min9120742, 2019.

Egger, M., Riedinger, N., Mogollón, J. M., and Jørgensen, B. B.: Global diffusive fluxes of methane in marine sediments, Nat. Geosci., 11, 421–425, https://doi.org/10.1038/s41561-018-0122-8, 2018.

Emerson, S. and Hedges, J. I.: Processes controlling the organic carbon content of open ocean sediments, Paleoceanography, 3, 621–634, https://doi.org/10.1029/PA003i005p00621, 1988.

Eyre, B. D., Cyronak, T., Drupp, P., De Carlo, E. H., Sachs, J. P., and Andersson, A. J.: Coral reefs will transition to net dissolving before end of century, Science, 359, 908–911, https://doi.org/10.1126/science.aao1118, 2018.

Fallati, L., Saponari, L., Savini, A., Marchese, F., Corselli, C., and Galli, P.: Multi-Temporal UAV Data and Object-Based Image Analysis (OBIA) for Estimation of Substrate Changes in a Post-Bleaching Scenario on a Maldivian Reef, Remote Sens., 12, 2093, https://doi.org/10.3390/rs12132093, 2020.

Fallati, L., Panieri, G., Argentino, C., Varzi, A. G., Bünz, S., and Savini, A.: Characterizing Håkon Mosby Mud Volcano (Barents Sea) cold seep systems by combining ROV-based acoustic data and underwater photogrammetry, Front. Mar. Sci., 10, 1–15, https://doi.org/10.3389/fmars.2023.1269197, 2023.

Ferré, B., Jansson, P. G., Moser, M., Serov, P., Portnov, A., Graves, C. A., Panieri, G., Gründger, F., Berndt, C., Lehmann, M. F., and Niemann, H.: Reduced methane seepage from Arctic sediments during cold bottom-water conditions, Nat. Geosci., 13, 144–148, https://doi.org/10.1038/s41561-019-0515-3, 2020.

Ferré, B., Panieri, G., Argentino, C., Sert, M. F., Stetzler, M., Fallati, L., Dills, M. S., Petters, S., Rohan, T., Barreyre, T., Lien, M. E., Kutti, T., Corrales, J., Kjær, M., Ting, R., Bojesen, M. D., Walta, A., and Jensen, S.: CAGE22-3 Cruise Report: EMAN7 cruise, CAGE – Cent. Arct. Gas Hydrate Environ. Clim. Rep. Ser., 10, https://doi.org/10.7557/cage.6760, 2022.

Ferré, B., Barreyre, T., Bünz, S., Argentino, C., Corrales-Guerrero, J., Dølven, K. O., Stetzler, M., Fallati, L., Sert, M. F., Panieri, G., Rastrick, S., Kutti, T., and Moser, M.: Contrasting Methane Seepage Dynamics in the Hola Trough Offshore Norway: Insights From Two Different Summers, J. Geophys. Res. Oceans, 129, e2024JC020949, https://doi.org/10.1029/2024JC020949, 2024.

Fischer, D., Sahling, H., Nöthen, K., Bohrmann, G., Zabel, M., and Kasten, S.: Interaction between hydrocarbon seepage, chemosynthetic communities, and bottom water redox at cold seeps of the Makran accretionary prism: Insights from habitat-specific pore water sampling and modeling, Biogeosciences, 9, 2013–2031, https://doi.org/10.5194/bg-9-2013-2012, 2012.

Foley, N. S., Van Rensburg, T. M., and Armstrong, C. W.: The ecological and economic value of cold-water coral ecosystems, Ocean Coast. Manag., 53, 313–326, https://doi.org/10.1016/j.ocecoaman.2010.04.009, 2010.

Fosså, J. H., Mortensen, P. B., and Furevik, D. M.: The deep-water coral Lophelia pertusa in Norwegian waters: Distribution and fishery impacts, Hydrobiologia, 471, 1–12, https://doi.org/10.1023/A:1016504430684, 2002.

Foucher, J. P., Westbrook, G. K., Boetius, A., Ceramicola, S., Dupré, S., Mascle, J., Mienert, J., Pfannkuche, O., Pierre, C., and Praeg, D.: Cold Seep Ecosystems Structure and Drivers of Cold Seep Ecosystems, Oceanography, 22, 92–109, 2007.

Freiwald, A.: Cold-Water Coral Reefs, in: Encyclopedia of Modern Coral Reefs, edited by: Hopley, D., Springer Netherlands, Dordrecht, 225–229, https://doi.org/10.1007/978-90-481-2639-2_68, 2011.

Garcia-Tigreros, F., Leonte, M., Ruppel, C. D., Ruiz-Angulo, A., Joung, D. J., Young, B., and Kessler, J. D.: Estimating the Impact of Seep Methane Oxidation on Ocean pH and Dissolved Inorganic Radiocarbon Along the U.S. Mid-Atlantic Bight, J. Geophys. Res. Biogeosciences, 126, e2019JG005621, https://doi.org/10.1029/2019JG005621, 2021.

Ghosh, A., Mazumdar, A., Sadique, Mohd., Peketi, A., Zatale, A., Sivan, K., Pillai, S. R., and Sparsh, A.: Chemosynthetic Organic Matter Reveals a Protracted Episode of Past Methane Seepage Activities at a Newly Discovered Cold Seep Site (Mannar Basin) Off the East Coast of India, Geophys. Res. Lett., 52, e2025GL116435, https://doi.org/10.1029/2025GL116435, 2025.

Gilbert, J. A., Jansson, J. K., and Knight, R.: The Earth Microbiome project: successes and aspirations, BMC Biol., 12, 69, https://doi.org/10.1186/s12915-014-0069-1, 2014.

Girard, F., Sarrazin, J., and Olu, K.: Impacts of an Eruption on Cold-Seep Microbial and Faunal Dynamics at a Mud Volcano, Front. Mar. Sci., 7, 241, https://doi.org/10.3389/fmars.2020.00241, 2020.

Greinert, J.: Monitoring temporal variability of bubble release at seeps: The hydroacoustic swath system GasQuant, J. Geophys. Res. Oceans, 113, 2007JC004704, https://doi.org/10.1029/2007JC004704, 2008.

Gruber, N. and Galloway, J. N.: An Earth-system perspective of the global nitrogen cycle, Nature, 451, 293–296, https://doi.org/10.1038/nature06592, 2008.

Gründger, F., Carrier, V., Svenning, M. M., Panieri, G., Vonnahme, T. R., Klasek, S., and Niemann, H.: Methane-fuelled biofilms predominantly composed of methanotrophic ANME-1 in Arctic gas hydrate-related sediments, Sci. Rep., 9, 1–10, https://doi.org/10.1038/s41598-019-46209-5, 2019.

Guezennec, J., Ortega-Morales, O., Raguenes, G., and Geesey, G.: Bacterial colonization of artificial substrate in the vicinity of deep-sea hydrothermal vents, FEMS Microbiol. Ecol., 26, 89–99, https://doi.org/10.1111/j.1574-6941.1998.tb00495.x, 1998.

Hasegawa, H., Kita, I., Tsukamoto, S., Chiyonobu, S., and Kuwahara, Y.: Synchronous Changes of Nitrogen and Carbon Isotopic Ratios and Nannoplankton Assemblage in Marine Sediments off Peru at 250 ka: A Role of Phytoplankton in Primary Ocean Productivity, Open J. Geol., 03, 113–120, https://doi.org/10.4236/ojg.2013.32015, 2013.

Hauri, C., Irving, B., Hayes, D., Abdi, E., Kemme, J., Kinski, N., and McDonnell, A. M. P.: Expanding seawater carbon dioxide and methane measuring capabilities with a Seaglider, Ocean Sci., 20, 1403–1421, https://doi.org/10.5194/os-20-1403-2024, 2024.

Hay, G. J. and Castilla, G.: Geographic Object-Based Image Analysis (GEOBIA): A new name for a new discipline, in: Object-Based Image Analysis, edited by: Blaschke, T., Lang, S., and Hay, G. J., Springer Berlin Heidelberg, Berlin, Heidelberg, 75–89, https://doi.org/10.1007/978-3-540-77058-9_4, 2008.

Hensen, C., Zabel, M., Pfeifer, K., Schwenk, T., Kasten, S., Riedinger, N., Schulz, H. D., and Boetius, A.: Control of sulfate pore-water profiles by sedimentary events and the significance of anaerobic oxidation of methane for the burial of sulfur in marine sediments, Geochim. Cosmochim. Acta, 67, 2631–2647, https://doi.org/10.1016/S0016-7037(03)00199-6, 2003.

Hilário, A., Capa, M., Dahlgren, T. G., Halanych, K. M., Little, C. T. S., Thornhill, D. J., Verna, C., and Glover, A. G.: New Perspectives on the Ecology and Evolution of Siboglinid Tubeworms, PLoS ONE, 6, e16309, https://doi.org/10.1371/journal.pone.0016309, 2011.

Hilmi, N., Allemand, D., Dupont, S., Safa, A., Haraldsson, G., Nunes, P. A. L. D., Moore, C., Hattam, C., Reynaud, S., Hall-Spencer, J. M., Fine, M., Turley, C., Jeffree, R., Orr, J., Munday, P. L., and Cooley, S. R.: Towards improved socio-economic assessments of ocean acidification's impacts, Mar. Biol., 160, 1773–1787, https://doi.org/10.1007/s00227-012-2031-5, 2013.

Hossain, M. D. and Chen, D.: Segmentation for Object-Based Image Analysis (OBIA): A review of algorithms and challenges from remote sensing perspective, ISPRS J. Photogramm. Remote Sens., 150, 115–134, https://doi.org/10.1016/j.isprsjprs.2019.02.009, 2019.

Hovland, M.: Do carbonate reefs form due to fluid seepage?, Terra Nova, 2, 8–18, https://doi.org/10.1111/j.1365-3121.1990.tb00031.x, 1990.

Hovland, M.: Deep-water Coral Reefs, Springer Netherlands, Dordrecht, https://doi.org/10.1007/978-1-4020-8460-7, 2008a.

Hovland, M.: Deep-water coral reefs: unique biodiversity hot-spots, Springer Praxis publ, New York Chichester, 2008b.

Hovland, M. and Thomsen, E.: Cold-water corals - Are they hydrocarbon seep related?, Mar. Geol., 137, 159–164, https://doi.org/10.1016/S0025-3227(96)00086-2, 1997.

Hu, Y., Feng, D., Peng, Y., Peckmann, J., Kasten, S., Wang, X., Liang, Q., Wang, H., and Chen, D.: A prominent isotopic fingerprint of nitrogen uptake by anaerobic methanotrophic archaea, Chem. Geol., 558, 119972, https://doi.org/10.1016/j.chemgeo.2020.119972, 2020.

Husebø, Å., Nøttestad, L., Fosså, J. H., Furevik, D. M., and Jørgensen, S. B.: Distribution and abundance of fish in deep-sea coral habitats, Hydrobiologia, 471, 91–99, https://doi.org/10.1023/A:1016549203368, 2002.

Joye, S. B.: The Geology and Biogeochemistry of Hydrocarbon Seeps, Annu. Rev. Earth Planet. Sci., 48, 205–231, https://doi.org/10.1146/annurev-earth-063016-020052, 2020.

Judd, A., Noble-James, T., Golding, N., Eggett, A., Diesing, M., Clare, D., Silburn, B., Duncan, G., Field, L., and Milodowski, A.: The Croker Carbonate Slabs: extensive methane-derived authigenic carbonate in the Irish Sea—nature, origin, longevity and environmental significance, Geo-Mar. Lett., 40, 423–438, https://doi.org/10.1007/s00367-019-00584-0, 2020.

Judd, A. G. and Hovland, M.: Seabed fluid flow: the impact of geology, biology and the marine environment, 1–442 pp., https://doi.org/10.1007/s00254-004-1086-0., 2007.

Kalenitchenko, D., Dupraz, M., Le Bris, N., Petetin, C., Rose, C., West, N. J., and Galand, P. E.: Ecological succession leads to chemosynthesis in mats colonizing wood in sea water, ISME J., 10, 2246–2258, https://doi.org/10.1038/ismej.2016.12, 2016.

Kang, H., Won, E., Shin, K., and Yoon, H. I.: Organic carbon and nitrogen composition in the sediment of the Kara Sea, Arctic Ocean during the Last Glacial Maximum to Holocene times, Geophys. Res. Lett., 34, 2007GL030068, https://doi.org/10.1029/2007GL030068, 2007.

Karaca, D., Hensen, C., and Wallmann, K.: Controls on authigenic carbonate precipitation at cold seeps along the convergent margin off Costa Rica, Geochem. Geophys. Geosystems, 11, 1–19, https://doi.org/10.1029/2010GC003062, 2010.

Kasten, S., Zabel, M., Heuer, V., and Hensen, C.: Processes and Signals of Nonsteady-State Diagenesis in Deep-Sea Sediments and their Pore Waters, in: The South Atlantic in the Late Quaternary, https://doi.org/10.1007/978-3-642-18917-3_20, 2003.

Kienast, M., Higginson, M. J., Mollenhauer, G., Eglinton, T. I., Chen, M.-T., and Calvert, S. E.: On the sedimentological origin of down-core variations of bulk sedimentary nitrogen isotope ratios, Paleoceanography, 20, n/a-n/a, https://doi.org/10.1029/2004PA001081, 2005.

Kline, D. I., Teneva, L., Okamoto, D. K., Schneider, K., Caldeira, K., Miard, T., Chai, A., Marker, M., Dunbar, R. B., Mitchell, B. G., Dove, S., and Hoegh-Guldberg, O.: Living coral tissue slows skeletal dissolution related to ocean acidification, Nat. Ecol. Evol., 3, 1438–1444, https://doi.org/10.1038/s41559-019-0988-x, 2019.

Knies, J.: Nitrogen Isotope Evidence for Changing Arctic Ocean Ventilation Regimes During the Cenozoic, Geophys. Res. Lett., 49, 1–8, https://doi.org/10.1029/2022GL099512, 2022.

Knies, J. and Martinez, P.: Organic matter sedimentation in the western Barents Sea region: Terrestrial and marine contribution based on isotopic composition and organic nitrogen content, Nor. Geol. Tidsskr., 89, 79–89, 2009.

Knies, J., Brookes, S., and Schubert, C. J.: Re-assessing the nitrogen signal in continental margin sediments: New insights from the high northern latitudes, Earth Planet. Sci. Lett., 253, 471–484, https://doi.org/10.1016/j.epsl.2006.11.008, 2007.

Kurth, J. M., Smit, N. T., Berger, S., Schouten, S., Jetten, M. S. M., and Welte, C. U.: Anaerobic methanotrophic archaea of the ANME-2d clade feature lipid composition that differs from other ANME archaea, FEMS Microbiol. Ecol., 95, fiz082, https://doi.org/10.1093/femsec/fiz082, 2019.

Lapham, L. L., Lloyd, K. G., Fossing, H., Flury, S., Jensen, J. B., Alperin, M. J., Rehder, G., Holzhueter, W., Ferdelman, T., and Jørgensen, B. B.: Methane leakage through the sulfate–methane transition zone of the Baltic seabed, Nat. Geosci., 17, 1277–1283, https://doi.org/10.1038/s41561-024-01594-z, 2024.

Lee, D. H., Lee, Y. M., Kim, J. H., Jin, Y. K., Paull, C., Niemann, H., Kim, J. H., and Shin, K. H.: Discriminative biogeochemical signatures of methanotrophs in different chemosynthetic habitats at an active mud volcano in the Canadian Beaufort Sea, Sci. Rep., 9, 1–13, https://doi.org/10.1038/s41598-019-53950-4, 2019.

Levin, L. a: Ecology of Cold Seep Sediments : Interactions of Fauna With Flow , Chemistry and Microbes, Oceanogr. Mar. Biol. Annu. Rev., 43, 1–46, https://doi.org/doi:10.1201/9781420037449.ch1, 2005.

Levin, L. A., Baco, A. R., Bowden, D. A., Colaco, A., Cordes, E. E., Cunha, M. R., Demopoulos, A. W. J. J., Gobin, J., Grupe, B. M., Le, J., Metaxas, A., Netburn, A. N., Rouse, G. W., Thurber, A. R., Tunnicliffe, V., Van Dover, C. L., Vanreusel, A., and Watling, L.: Hydrothermal Vents and Methane Seeps: Rethinking the Sphere of Influence, Front. Mar. Sci., 3, 1–23, https://doi.org/10.3389/fmars.2016.00072, 2016.

Liebetrau, V., Eisenhauer, A., and Linke, P.: Cold seep carbonates and associated cold-water corals at the Hikurangi Margin, New Zealand: New insights into fluid pathways, growth structures and geochronology, Mar. Geol., 272, 307–318, https://doi.org/10.1016/j.margeo.2010.01.003, 2010.

Lim, A., Wheeler, A. J., Price, D. M., O'Reilly, L., Harris, K., and Conti, L.: Influence of benthic currents on cold-water coral habitats: a combined benthic monitoring and 3D photogrammetric investigation, Sci. Rep., 10, 19433, https://doi.org/10.1038/s41598-020-76446-y, 2020.

Liu, C., Cui, Y., Li, X., and Yao, M.: microeco: an R package for data mining in microbial community ecology, FEMS Microbiol. Ecol., 97, fiaa255, https://doi.org/10.1093/femsec/fiaa255, 2021.

Madigan, M. T., Bender, K. S., Buckley, D. H., Sattley, M. W., and Stahl, D. A.: Brock Biology of Microorganisms, Global Edition, Pearson Education Limited, 2017.

Meyers, P. A.: Preservation of elemental and isotopic source identification of sedimentary organic matter, Chem. Geol., 114, 289–302, https://doi.org/10.1016/0009-2541(94)90059-0, 1994.

Meyers, P. A.: Organic geochemical proxies of paleoceanographic, paleolimnologic, and paleoclimatic processes, Org. Geochem., 27, 213–250, https://doi.org/10.1016/S0146-6380(97)00049-1, 1997.

Milkov, A. V. and Etiope, G.: Revised genetic diagrams for natural gases based on a global dataset of >20,000 samples, Org. Geochem., 125, 109–120, https://doi.org/10.1016/j.orggeochem.2018.09.002, 2018.

Millero, F. J.: Chemical Oceanography, 0 ed., CRC Press, https://doi.org/10.1201/9780429258718, 2005.

Minami, H. and Tatsumi, K.: Possible variation in methane flux caused by gas hydrate formation on the northeastern continental slope off Sakhalin, 525–534, https://doi.org/10.1007/s00367-012-0287-x, 2012.

Montes-Herrera, J. C., Hill, N., Cummings, V. J., Johnstone, G. J., Stark, J. S., and Lucieer, V.: Remote sensing of Antarctic polychaete reefs (Serpula narconensis): reproducible workflows for quantifying benthic structural complexity with action cameras, remotely operated vehicles and structure-from-motion photogrammetry, Remote Sens. Ecol. Conserv., 10, 72–90, https://doi.org/10.1002/rse2.358, 2024.

Naidu, A. S., Cooper, L. W., Finney, B. P., Macdonald, R. W., Alexander, C., and Semiletov, I. P.: Organic carbon isotope ratios (δ 13 C) of Arctic Amerasian Continental shelf sediments, Int. J. Earth Sci., 89, 522–532, https://doi.org/10.1007/s005310000121, 2000.

Niemann, H., Linke, P., Knittel, K., MacPherson, E., Boetius, A., Brückmann, W., Larvik, G., Wallmann, K., Schacht, U., Omoregie, E., Hilton, D., Brown, K., and Rehder, G.: Methane-Carbon Flow into the Benthic Food Web at Cold Seeps – A Case Study from the Costa Rica Subduction Zone, PLoS ONE, 8, e74894, https://doi.org/10.1371/journal.pone.0074894, 2013.

Noffke, N.: Geobiology: Microbial Mats in Sandy Deposits from the Archean Era to Today, Springer Berlin Heidelberg, Berlin, Heidelberg, https://doi.org/10.1007/978-3-642-12772-4, 2010.

Oksanen, J., Simpson, G. L., Blanchet, F. G., Kindt, R., Legendre, P., Minchin, P. R., O'Hara, R. B., Solymos, P., Stevens, M. H. H., Szoecs, E., Wagner, H., Barbour, M., Bedward, M., Bolker, B., Borcard, D., Borman, T., Carvalho, G., Chirico, M., De Caceres, M., Durand, S., Evangelista, H. B. A., FitzJohn, R., Friendly, M., Furneaux, B., Hannigan, G., Hill, M. O., Lahti, L., Martino, C., McGlinn, D., Ouellette, M.-H., Ribeiro Cunha, E., Smith, T., Stier, A., Ter Braak, C. J. F., and Weedon, J.: vegan: Community Ecology Package, https://doi.org/10.32614/CRAN.package.vegan, 2001.

Osman, E. O., Vohsen, S. A., Girard, F., Cruz, R., Glickman, O., Bullock, L. M., Anderson, K. E., Weinnig, A. M., Cordes, E. E., Fisher, C. R., and Baums, I. B.: Capacity of deep-sea corals to obtain nutrition from cold seeps aligned with microbiome reorganization, Glob. Change Biol., 29, 189–205, https://doi.org/10.1111/gcb.16447, 2023.

Ottesen, D., Dowdeswell, J. A., and Rise, L.: Submarine landforms and the reconstruction of fast-flowing ice streams within a large Quaternary ice sheet: The 2500-km-long Norwegian-Svalbard margin (57°–80°N), Geol. Soc. Am. Bull., 117, 1033, https://doi.org/10.1130/B25577.1, 2005.

Pan, J., Perillo, V. L., and Cuadrado, D. G.: Quantification of microbial mat response to physical disruption in siliciclastic sediments, Estuar. Coast. Shelf Sci., 230, 106434, https://doi.org/10.1016/j.ecss.2019.106434, 2019.

Panieri, G., Argentino, C., Ramalho, S. P., Vulcano, F., Savini, A., Fallati, L., Brekke, T., Galimberti, G., Riva, F., Balsa, J., Eilertsen, M. H., Stokke, R., Steen, I. H., Sahy, D., Kalenitchenko, D., Büenz, S., and Mattingsdal, R.: An Arctic natural oil seep investigated from space to the seafloor, Sci. Total Environ., 907, 167788, https://doi.org/10.1016/j.scitotenv.2023.167788, 2024.

Phrampus, B. J., Lee, T. R., and Wood, W. T.: A Global Probabilistic Prediction of Cold Seeps and Associated SEAfloor FLuid Expulsion Anomalies (SEAFLEAs), Geochem. Geophys. Geosystems, 21, https://doi.org/10.1029/2019GC008747, 2020.

Pirlet, H., Wehrmann, L. M., Foubert, A., Brunner, B., Blamart, D., De Mol, L., Van Rooij, D., Dewanckele, J., Cnudde, V., Swennen, R., Duyck, P., and Henriet, J.: Unique authigenic mineral assemblages reveal different diagenetic histories in two neighbouring cold-water coral mounds on Pen Duick Escarpment, Gulf of Cadiz, Sedimentology, 59, 578–604, https://doi.org/10.1111/j.1365-3091.2011.01267.x, 2012.

Price, D. M., Robert, K., Callaway, A., Lo Lacono, C., Hall, R. A., and Huvenne, V. A. I.: Using 3D photogrammetry from ROV video to quantify cold-water coral reef structural complexity and investigate its influence on biodiversity and community assemblage, Coral Reefs, 38, 1007–1021, https://doi.org/10.1007/s00338-019-01827-3, 2019.

Probst, A. J., Weinmaier, T., Raymann, K., Perras, A., Emerson, J. B., Rattei, T., Wanner, G., Klingl, A., Berg, I. A., Yoshinaga, M., Viehweger, B., Hinrichs, K.-U., Thomas, B. C., Meck, S., Auerbach, A. K., Heise, M., Schintlmeister, A.,

Schmid, M., Wagner, M., Gribaldo, S., Banfield, J. F., and Moissl-Eichinger, C.: Biology of a widespread uncultivated archaeon that contributes to carbon fixation in the subsurface, Nat. Commun., 5, 5497, https://doi.org/10.1038/ncomms6497, 2014.

Quast, C., Pruesse, E., Yilmaz, P., Gerken, J., Schweer, T., Yarza, P., Peplies, J., and Glöckner, F. O.: The SILVA ribosomal RNA gene database project: improved data processing and web-based tools, Nucleic Acids Res., 41, D590-596, https://doi.org/10.1093/nar/gks1219, 2013.

R Core Team: R: A language and environment for statistical computing, 2021.

Rachold, V. and Hubberten, H.-W.: Carbon Isotope Composition of Particulate Organic Material in East Siberian Rivers, in: Land-Ocean Systems in the Siberian Arctic, edited by: Kassens, H., Bauch, H. A., Dmitrenko, I. A., Eicken, H., Hubberten, H.-W., Melles, M., Thiede, J., and Timokhov, L. A., Springer Berlin Heidelberg, Berlin, Heidelberg, 223–238, https://doi.org/10.1007/978-3-642-60134-7_21, 1999.

Riesch, R., Tobler, M., and Plath, M.: Hydrogen Sulfide-Toxic Habitats, in: Extremophile Fishes, edited by: Riesch, R., Tobler, M., and Plath, M., Springer International Publishing, Cham, 137–159, https://doi.org/10.1007/978-3-319-13362-1_7, 2015.

Rincon-Tomas, B., Duda, J. P., Somoza, L., Javier González, F., Schneider, D., Medialdea, T., Santofimia, E., López-Pamo, E., Madureira, P., Hoppert, M., and Reitner, J.: Cold-water corals and hydrocarbon-rich seepage in Pompeia Province (Gulf of Cádiz) - Living on the edge, Biogeosciences, 16, 1607–1627, https://doi.org/10.5194/bg-16-1607-2019, 2019.

Roberts, J. M., Wheeler, A., Freiwald, A., and Cairns, S.: Cold-Water Corals: The Biology and Geology of Deep-Sea Coral Habitats, 1st ed., Cambridge University Press, https://doi.org/10.1017/CBO9780511581588, 2009.

Robeson, M. S., O'Rourke, D. R., Kaehler, B. D., Ziemski, M., Dillon, M. R., Foster, J. T., and Bokulich, N. A.: RESCRIPt: Reproducible sequence taxonomy reference database management, PLOS Comput. Biol., 17, e1009581, https://doi.org/10.1371/journal.pcbi.1009581, 2021.

Ruttenberg, K. C. and Goñi, M. A.: Phosphorus distribution, C:N:P ratios, and δ13Coc in arctic, temperate, and tropical coastal sediments: tools for characterizing bulk sedimentary organic matter, Mar. Geol., 139, 123–145, https://doi.org/10.1016/S0025-3227(96)00107-7, 1997.

Sahling, H., Rickert, D., Lee, R. W., Linke, P., and Suess, E.: Macrofaunal community structure and sulfide flux at gas hydrate deposits from the Cascadia convergent margin, NE Pacific, Mar. Ecol. Prog. Ser., 231, 121–138, https://doi.org/10.3354/meps231121, 2002.

Sanna, G., Büscher, J. V., and Freiwald, A.: Cold-water coral framework architecture is selectively shaped by bottom current flow, Coral Reefs, 42, 483–495, https://doi.org/10.1007/s00338-023-02361-z, 2023.

Sauer, S., Knies, J., Lepland, A., Chand, S., Eichinger, F., and Schubert, C. J.: Hydrocarbon sources of cold seeps off the Vesterålen coast, northern Norway, Chem. Geol., 417, 371–382, https://doi.org/10.1016/j.chemgeo.2015.10.025, 2015.

Sauer, S., Crémière, A., Knies, J., Lepland, A., Sahy, D., Martma, T., Noble, S. R., Schönenberger, J., Klug, M., and Schubert, C. J.: U-Th chronology and formation controls of methane-derived authigenic carbonates from the Hola trough seep area, northern Norway, Chem. Geol., 470, 164–179, https://doi.org/10.1016/j.chemgeo.2017.09.004, 2017.

Schneider, A., Panieri, G., Lepland, A., Consolaro, C., Crémière, A., Forwick, M., Johnson, J. E., Plaza-Faverola, A., Sauer, S., and Knies, J.: Methane seepage at Vestnesa Ridge (NW Svalbard) since the Last Glacial Maximum, Quat. Sci. Rev., 193, 98–117, https://doi.org/10.1016/j.quascirev.2018.06.006, 2018.

Schroeder, W. W.: Observations of Lophelia pertusa and the surficial geology at a deep-water site in the northeastern Gulf of Mexico, Hydrobiologia, 471, 29–33, https://doi.org/10.1023/A:1016580632501, 2002.

Seabrook, S., De Leo, F. C., and Thurber, A. R.: Flipping for Food: The Use of a Methane Seep by Tanner Crabs (Chionoecetes tanneri), Front. Mar. Sci., 6, 43, https://doi.org/10.3389/fmars.2019.00043, 2019.

Sen, A., Duperron, S., Hourdez, S., Piquet, B., Léger, N., Gebruk, A., Le Port, A. S., Svenning, M. M., and Andersen, A. C.: Cryptic frenulates are the dominant chemosymbiotrophic fauna at Arctic and high latitude Atlantic cold seeps, PLoS ONE, 13, https://doi.org/10.1371/journal.pone.0209273, 2018a.

Sen, A., Aström, E. K. L., Hong, W. L., Portnov, A., Waage, M., Serov, P., Carroll, M. L., and Carroll, J. L.: Geophysical and geochemical controls on the megafaunal community of a high Arctic cold seep, Biogeosciences, 15, 4533–4559, https://doi.org/10.5194/bg-15-4533-2018, 2018b.

Sen, A., Himmler, T., Hong, W. L., Chitkara, C., Lee, R. W., Ferré, B., Lepland, A., and Knies, J.: Atypical biological features of a new cold seep site on the Lofoten-Vesterålen continental margin (northern Norway), Sci. Rep., 9, 1–14, https://doi.org/10.1038/s41598-018-38070-9, 2019.

Sert, M. F., Bernstein, H. C., Dølven, K. O., Petters, S., Kekäläinen, T., Jänis, J., Corrales-Guerrero, J., and Ferré, B.: Cold Seeps and Coral Reefs in Northern Norway: Carbon Cycling in Marine Ecosystems With Coexisting Features, J. Geophys. Res. Biogeosciences, 130, e2024JG008475, https://doi.org/10.1029/2024JG008475, 2025.

Southward, E. C., Schulze, A., and Gardiner, S. L.: Pogonophora (Annelida): form and function, in: Morphology, Molecules, Evolution and Phylogeny in Polychaeta and Related Taxa, vol. 179, edited by: Bartolomaeus, T. and Purschke, G., Springer-Verlag, Berlin/Heidelberg, 227–251, https://doi.org/10.1007/1-4020-3240-4_13, 2005.

Stock, L., Wegener, G., Wang, Y., Zander, Y., and Elvert, M.: Marine Cold Seep ANME -2/ SRB Consortia Produce Their Lipid Biomass From Inorganic Carbon, Environ. Microbiol., 27, e70213, https://doi.org/10.1111/1462-2920.70213, 2025.

Sundahl, H., Buhl-Mortensen, P., and Buhl-Mortensen, L.: Distribution and Suitable Habitat of the Cold-Water Corals Lophelia pertusa, Paragorgia arborea, and Primnoa resedaeformis on the Norwegian Continental Shelf, Front. Mar. Sci., 7, 213, https://doi.org/10.3389/fmars.2020.00213, 2020.

Szymczycha, B., Diak, M., Hong, W.-L., Böttcher, M. E., Lepland, A., Makuch, P., Ten Hietbrink, S., Saghravani, S. R., Sen, A., Winogradow, A., and Silberberger, M. J.: Submarine groundwater discharge and gas hydrate dissociation fuel organic matter formation in Arctic fjord sediments, Mar. Chem., 273, 104570, https://doi.org/10.1016/j.marchem.2025.104570, 2025.

Thurber, A. R., Levin, L. A., Rowden, A. A., Sommer, S., Linke, P., and Kröger, K.: Microbes, macrofauna, and methane: A novel seep community fueled by aerobic methanotrophy, Limnol. Oceanogr., 58, 1640–1656, https://doi.org/10.4319/lo.2013.58.5.1640, 2013.

Tobler, M., Passow, C. N., Greenway, R., Kelley, J. L., and Shaw, J. H.: The Evolutionary Ecology of Animals Inhabiting Hydrogen Sulfide–Rich Environments, Annu. Rev. Ecol. Evol. Syst., 47, 239–262, https://doi.org/10.1146/annurev-ecolsys-121415-032418, 2016.

Tseng, Y., Smrzka, D., Lin, S., Schröder-Ritzrau, A., Frank, N., and Bohrmann, G.: Authigenic Carbonate Precipitation at Yam Seep Controlled by Continuous Fracturing and Uplifting of Four-Way Closure Ridge Offshore SW Taiwan, Geochem. Geophys. Geosystems, 24, https://doi.org/10.1029/2022GC010652, 2023.

Vuillemin, A., Coskun, Ö. K., and Orsi, W. D.: Microbial Activities and Selection from Surface Ocean to Subseafloor on the Namibian Continental Shelf, Appl. Environ. Microbiol., 88, e00216-22, https://doi.org/10.1128/aem.00216-22, 2022.

Wada, E.: Nitrogen isotope fractionation and its significance in biogeochemical processes occurring in marine environments., Isot. Mar. Chem., 375–398, 1980.

Wegener, G., Niemann, H., Elvert, M., Hinrichs, K.-U., and Boetius, A.: Assimilation of methane and inorganic carbon by microbial communities mediating the anaerobic oxidation of methane, Environ. Microbiol., 10, 2287–2298, https://doi.org/10.1111/j.1462-2920.2008.01653.x, 2008.

Whiticar, M. J.: The Biogeochemical Methane Cycle, in: Hydrocarbons, Oils and Lipids: Diversity, Origin, Chemistry and Fate, Springer International Publishing, Cham, 1–78, https://doi.org/10.1007/978-3-319-54529-5_5-1, 2020.

Wisshak, M., Schönberg, C. H. L., Form, A., and Freiwald, A.: Ocean Acidification Accelerates Reef Bioerosion, PLoS ONE, 7, e45124, https://doi.org/10.1371/journal.pone.0045124, 2012.

Xu, A., Chen, Z., Qu, Y., Tian, Y., Shu, C., Zheng, X., Li, G., Yan, W., and Zhao, M.: Cold-water corals in a cold seep area on the northern continental slopes of the South China sea and their isotopic characteristics, Deep Sea Res. Part Oceanogr. Res. Pap., 152, 103043, https://doi.org/10.1016/j.dsr.2019.05.003, 2019.

Yao, H., Niemann, H., and Panieri, G.: Multi-proxy approach to unravel methane emission history of an Arctic cold seep, Quat. Sci. Rev., 244, 106490, https://doi.org/10.1016/j.quascirev.2020.106490, 2020.

Yilmaz, P., Parfrey, L. W., Yarza, P., Gerken, J., Pruesse, E., Quast, C., Schweer, T., Peplies, J., Ludwig, W., and Glöckner, F. O.: The SILVA and "All-species Living Tree Project (LTP)" taxonomic frameworks, Nucleic Acids Res., 42, D643–D648, https://doi.org/10.1093/nar/gkt1209, 2014.

Yoshinaga, M. Y., Holler, T., Goldhammer, T., Wegener, G., Pohlman, J. W., Brunner, B., Kuypers, M. M. M., Hinrichs, K., and Elvert, M.: Carbon isotope equilibration during sulphate-limited anaerobic oxidation of methane, 7, https://doi.org/10.1038/NGEO2069, 2014.

Zhang, X., Walz, P. M., Kirkwood, W. J., Hester, K. C., Ussler, W., Peltzer, E. T., and Brewer, P. G.: Development and deployment of a deep-sea Raman probe for measurement of pore water geochemistry, Deep-Sea Res. Part Oceanogr. Res. Pap., 57, 297–306, https://doi.org/10.1016/j.dsr.2009.11.004, 2010.

Zhang, X., Kirkwood, W. J., Hester, K. C., Walz, P. M., Ussler, W., Peltzer, E. T., Shane, F., and Brewer, P. G.: In situ Raman probe for quantitative observation of sediment pore waters in the Deep Ocean - Development and applications, OCEANS 2011 IEEE - Spain, 1–8, https://doi.org/10.1109/Oceans-Spain.2011.6003421, 2011.